https://doi.org/10.1070/RCR4897

Self-assembled interface monolayers for organic and hybrid electronics

Alexey S. Sizov, Elena V. Agina, Sergey A. Ponomarenko

Enikolopov Institute of Synthetic Polymeric Materials, Russian Academy of Sciences, ul. Profsoyuznaya 70, 117393 Moscow, Russian Federation

The state of the art in the field of self-assembled organic interface monolayers widely used in organic and hybrid electronics is analyzed and the results obtained are summarized. Recent advances in full and local substrate modification using interface layers are considered in detail. Examples of the most successful applications of interface monolayers as monolayer dielectrics, modifiers of the work function and adhesion promoters are given. The advantages of utilizing interface monolayers at semiconductor/dielectric interfaces and for modifying the semiconductor surface are demonstrated. Specific features of formation of nanostructured surfaces including those used in biosensoric applications are outlined.
The bibliography includes 139 references.

Contents

1. Introduction 1221
2. Self-assembled interface monolayers for monolayer and hybrid dielectrics 1223
3. Self-assembled interface layers as adhesion promoters 1227
4. Self-assembled interface monolayers for nanostructured surface formation 1230
5. Self-assembled interface monolayers at semiconductor/dielectric interface in field-effect transistors 1232
6. Self-assembled interface monolayers as work function modifiers 1235
7. Self-assembled interface monolayers for surface modification of organic semiconductors 1239
8. Self-assembled interface monolayers for applications in biosensors 1241
9. Conclusion 1243

The list of notations and abbreviations used in this review is as follows:

AFM — atomic force microscopy,
APTS — (3-aminopropyl)trimethoxysilane,
C — capacitance of dielectric layer,
CA — contact angle
CV — cyclic voltammetry,
(E)PEI — (ethoxylated) polyethyleneimine,
FET — field-effect transistor,
FTS — (tridecafluoro-1,1,2,2-tetrahydrooctyl)trisilane,
FTES — (tridecafluoro-1,1,2,2-tetrahydrooctyl)triethoxysilane,
HMDS — hexamethyldisilazane,
I_d — drain current,
I_g — gate current,
ITO — indium tin oxide,
MPTS — (3-mercaptopropyl)trimethoxysilane,
ODPA — n-octadecylphosphonic acid,
ODTS — n-octadecyltrichlorosilane,
n-ODTM — n-octadecyltrimethoxysilane,
OFET — organic field-effect transistor,
OLED — organic light-emitting diode,

A.S.Sizov. Candidate of Chemical Sciences; currently at InnovationLab GmbH, Speyerer Str. 4, 69115 Heidelberg, Germany.
Telephone: +7(495)332 – 5847, e-mail: alexey.sizov@outlook.com
Current research interests: design of innovative organic microelectronics devices based on conjugated oligomers, including organic field-effect transistors, organic integrated circuits, gas sensors; search for methods of frabrication of thin films with specified optoelectronic properties based on organic compounds; characterization of functional layers of organic electronics devices using various methods.
E.V.Agina. Candidate of Chemical Sciences, Leading Researcher at ISPM RAS.
Telephone: +7(495)332 – 5847, e-mail: agina@ispm.ru
Current research interests: molecular and supramolecular self-assembly in bulk and in thin films of linear and branched carbosilane-siloxanes with various functional, in particular, mesogenic and semiconducting groups; search for efficient methods for fabrication of highly organized (including 2D) nanomaterials with specified structure and properties based on organic semiconductors.
S.A.Ponomarenko. Corresponding Member of the Russian Academy of Sciences, Doctor of Chemical Sciences, Director of ISPM RAS.
Telephone: +7(495)332 – 5876, e-mail: ponomarenko@ispm.ru
Current research interests: molecular design and synthesis of advanced conjugated organic and organosilicon structures (first of all, based on thiophene and silicon) with high charge carrier mobility, effective luminescence, good solution processability, oxidative and thermal stability and other properties necessary to design novel materials and technologies for organic electronics and nanophotonics.

Received 26 March 2019
Translation: A.M.Raevskiy

© 2019 Uspekhi Khimii, Russian Academy of Sciences and Turpion Ltd.

OMPMS — oligo[(3-mercaptopropyl)(methoxy)siloxane],
OTS — n-octyltrichlorosilane,
p — pressure,
p_0 — saturated vapour pressure,
PAA — polyacrylic acid,
PDMS — polydimethylsiloxane,
PEN — polyethylene naphthalate,
PET — polyethylene terephthalate,
PI — polyimide,
q — elementary charge,
SAIM — self-assembled interface monolayer,
SC — semiconductor,
SCT — spin coating technique,
SKPM — scanning Kelvin probe microscopy,
TAA — triarylamine,
TEDA — *N*-[3-(triethoxysilyl)propyl]ethane-1,2-diamine,
UPS — ultraviolet photoelectron/photoemission spectroscopy,
V_{ds} —drain – source voltage,
V_g — gate voltage,
V_{sf} — local surface potential,
V_t — threshold voltage,
XPS — X-ray photoelectron spectroscopy,
XRD — X-ray diffraction,
μ — charge carrier mobility,
τ — time constant,
σ — conductivity.

1. Introduction

Organic electronics is a rapidly progressing field of science and technology at the intersection of chemistry, physics and materials science. The application of functional materials based on conjugated organic compounds offers prospects for the design of advanced optoelectronic devices characterized by low cost, light weight, flexible architecture and optical transparency. Fabrication of electronic devices from organic components only is a challenge and therefore real organic electronic devices are made of both organic and inorganic materials. Combining organic and inorganic (*e.g.*, silicon, a typical electronic material) semiconductor components in a single device makes the design of interface layers highly topical. Such layers are a kind of auxiliary functional units that facilitate proper and efficient operation of electronic devices.

An efficient strategy for fabrication of interface layers is to utilize their self-assembly from molecules. According to Whitesides and Grzybowski,[1] 'self-assembly is the autonomous organization of components into patterns or structures without human intervention'. In organic electronics, self-assembly of various functional layers of devices is widely used since this approach is characterized by high processability and energy efficiency.[2–5]

This review is devoted to self-assembled interface monolayers (SAIMs) in organic and hybrid electronic devices. Such layers make it possible to change the surface properties of materials, which is of crucial importance for the design of multilayer devices, in particular, organic field-effect transistors (OFETs), organic solar cells and organic light-emitting diodes (OLEDs). Self-assembled interface monolayers can be used to enhance the adhesion of conductive structures to substrates, dielectric or semiconductor layers.[6] As will be shown below, SAIMs often allow researchers to simultaneously solve a number of problems, *e.g.*, to change the surface energy of the substrate and thus to shift the OFET threshold voltage. It should be noted that various devices can efficiently operate without SAIMs and, strictly speaking, there is no need in the SAIMs in contrast to, *e.g.*, the dielectric layer. At the same time, this review concerns the state-of-the-art in practical applications of interface layers with the emphasis placed on demonstration of the idea that parameters of electronic devices can be significantly improved using SAIMs.

A variety of review articles concerning interface layers for organic and unconventional inorganic electronics are available. The review by DiBenedetto *et al.*[7] published in 2009 is the closest in subject to this one; however, rapid recent progress in organic electronics accompanied by publication of a huge number of impressive communications makes the present review topical. In some cases problems related to SAIMs were briefly outlined in the context of wider themes.[6,8] Besides, reviews on methods for modification of polymer films for printed electronics were published in 2018.[9,10] All these studies only partially overlap in topic with the present review.

It should be noted that the first studies on SAIMs date back to the 1940s and a rather large number of relevant reviews have been reported to date.[11–13] In this review we focused on the application of SAIMs in the design of microelectronic devices for organic and hybrid electronics. Using published data, we will analyze correlations between the structure of precursors for interface layers and macroscopic physical parameters responsible for efficient operation of electronic devices. Many publications analyzed here are related to field-effect transistors (FETs) since they are basic units for more complex devices, such as integrated circuits or sensors. Additional information on FETs can be gained from reviews devoted to advances in the design of organic FETs (OFETs).[5,14,15] In addition to the publications mentioned above, we will consider studies on the application of SAIMs in OLEDs[16] and solar cells.[17–19]

Possible applications of SAIMs include fabrication of monolayer and hybrid dielectrics, formation of multipurpose nanostructured surfaces including those demonstrating the properties of biosensors, change of the conductor (electrode) work function, shift of the OFET threshold voltage upon modification of the semiconductor/dielectric interface, doping of organic semiconductors during surface modification, reduction of the free energy of the surface, and enhancement of adhesion of conductive patterned structures to substrates and dielectric or semiconductor layers.

A typical structure of a SAIM precursor is shown in Fig. 1 *a*. The anchor (reactive) group forms a covalent bond with the substrate, the end group is responsible for the interaction with the functional layer that is formed above the SAIM, and the flexible spacer provides independent behaviour of the anchor and end groups and facilitates intra-layer self-assembly through, in particular, self-crystallization. The choice of the anchor group depends on the type of the surface modified. Traditionally used anchor groups include a phosphonic acid residue (for modification of Al compounds), chlorosilyl or alkoxyl groups (for modification of Si compounds), as

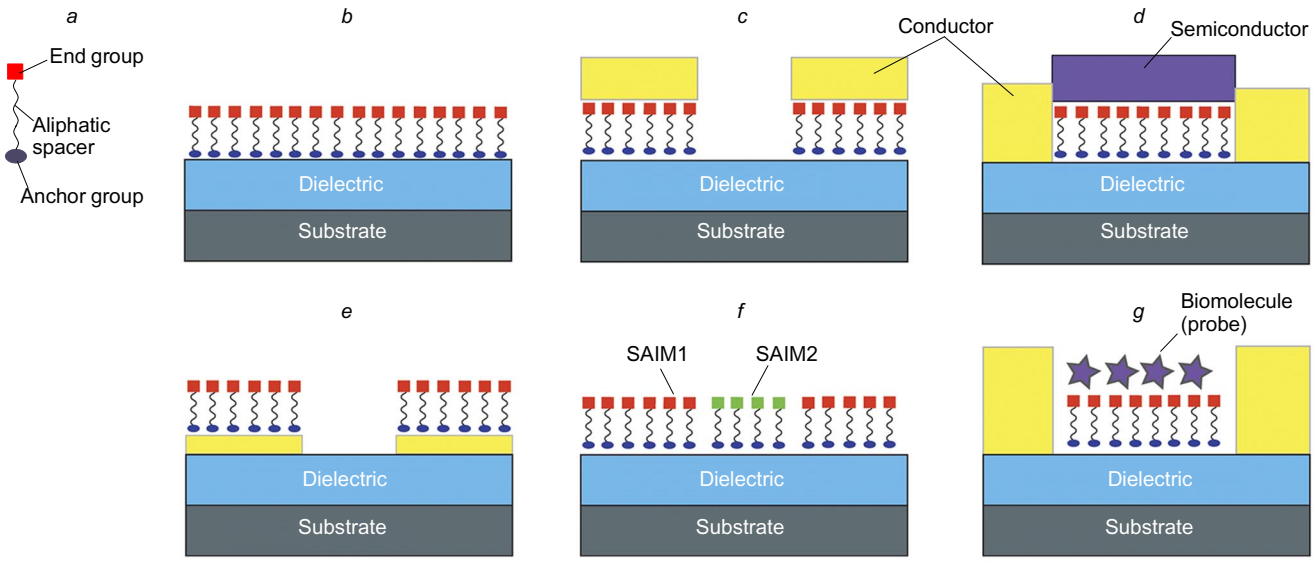


Figure 1. Structure of a compound used as SAIM precursor (*a*) and examples of topologies of microelectronic devices containing SAIMs: full (*b*) and local (*c*) modification of a dielectric using SAIM; SAIM at dielectric/semiconductor interface in FET (*d*); SAIM-modifed metallic electrodes (*e*); SAIMs for nanostructured surface formation (*f*); and SAIM for applications in biosensors (*g*).

well as thiols or their derivatives (for modification of Au compounds). The choice of the end groups is specified by the application field of the SAIM and by the structure of the functional layer atop the SAIM. Commonly used end groups include methyl, hydroxyl, carboxyl, amino, azido, thiol, phenyl (Ph), imidazole (Imi) as well as perfluorinated aromatic (C_6F_6) and triarylamino groups (Table 1). The end groups can (i) form covalent bonds with the upper-lying layer and thus ensure its adhesion to the substrate or the interaction with biomolecules, being responsible for the sensor properties, and (ii) control the roughness and hydrophilic-hydrophobic balance of the substrate, thus providing uniform (templated) layer-by-layer coating of the substrate. In addition, by varying the chemical structure of the end group one can (a) change the dipole moment of the SAIM and thus, in particular, change the FET threshold voltage and the electrode work function, (b) vary the sensor properties of the layer, *etc*. We believe that the choice of spacer is to a great extent determined by the commercial availability of reactants containing the necessary anchor and end groups. Conventional spacers include alkyl (C_2-C_{12}) or perfluoroalkyl fragments as well as polyacrylic acid, polyethyleneimine or diaryldiaza derivatives.

Table 1. Chemical structure of SAIMs depending on the type of the modified surface and on the application field.

Precursor for SAIM [a]		Substrate	Application
end group	anchor group		
CH_3, OH, SH, Ph, Imi	$PO(OH)_2$	Al (Al_2O_3)	Multilayer dielectrics
NH_2, SH, N_2	$PO(OH)_2$, $SiCl_3$, $Si(OAlk)_3$	Al (Al_2O_3), Si (SiO_2)	Adhesion promoters
NH_2, CH, CH_3, OH, SH, CF_3	$SiCl_3$, $Si(OAlk)_3$	Si (SiO_2)	Nanostructured surface
CH_3, CF_3, OH, PEI, TAA	$Si(OAlk)_3$, PEI, PAA	PEN, PI, PET	Changee of electrode work function
$OOC-C_6F_6$, COOH, OH, CH_3	$Si(OAlk)_3$, PEI, PAA	PEN, PI, PET	Biosensors

Note. Notations are as follows: PEI is polyethyleneimine, TAA is triarylamine, PAA is polyacrylic acid, PEN is polyethylene naphthalate, PET is polyethylene terephthalate and PI is polyimide.
[a] All SAIMs contain $(CH_2)_n$ or $(CF_2)_n$ ($n = 2-12$) units as spacers.

Typical topologies of microelectronic devices with SAIMs are presented in Fig. 1. The most widely used approach involves nonlocal modification of substrates (see Fig. 1 *b*) and thus allows one to change the surface energy of the substrate. The SAIM thus fabricated can be used in electronic devices as monolayer dielectric.[20] In addition, SAIMs to a great extent specify the overall process of organic film formation on modified substrates. Local modification of substrates using SAIMs can be employed to enhance the adhesion between conductive structures and substrates[21] (see Fig. 1 *c*) or to improve the electrical properties of organic semiconductors deposited onto the SAIM (see Fig. 1 *d*).[22] Yet another application of SAIMs involves modification of metallic electrodes to change the electrode work function and to improve the injection of charge carriers into the semiconductor functional layer of the device (see Fig. 1 *e*).[23] Self-assembled interface monolayers are also used for nanostructuring of substrate surface and subsequent formation of microelectronic devices on this surface (see Fig. 1 *f*). The review is completed with the Section devoted to application of SAIMs in biosensors, where the interface layer is utilized to form a target-specific receptor layer based on probe biomolecules (see Fig. 1 *g*). The potential application range of SAIM in organic and hybrid electronics is not limited to the given examples presented.

2. Self-assembled interface monolayers for monolayer and hybrid dielectrics

As mentioned above, SAIMs in organic and hybrid electronic devices are often responsible for several different functions. Examples are provided by monolayer dielectrics based on bifunctional organic compounds containing an anchor group to form a covalent bond with the substrate and an end group that interacts with a metal or organic semiconductor (see Fig. 1 *b*). Monolayer dielectrics are widely used for fabrication of low-voltage FETs since they allow one to decrease the gate dielectric thickness to a few nanometres and, as a consequence, to significantly increase its electrical capacitance. At the same time, the chemical structure of SAIMs to a great extent determines the surface roughness and wettability of the substrate for the semiconductor layer. Also, a nonzero dipole moment of the SAIM makes it possible to shift the FET threshold voltage over a wide range and to influence the charge carrier mobility, as was shown experimentally for various organic semiconductors.[20,24–27] Since charge carrier transport in FETs occurs in a thin semiconductor layer (layer thickness is 3 – 5 nm) at the interface with the dielectric, the interface layer specifies the electrical properties of the entire device. Thus, the design of precursors capable of forming monolayer dielectrics is an important problem in organic and hybrid electronics.

The key physical quantities characterizing the properties of monolayer dielectrics are as follows: contact angle (θ/deg), leakage current density [density of parasite current flowing through the SAIM per unit surface area (j/A cm^{-2})], breakdown field [maximum electric field at which the dielectric properties of a SAIM are retained (E_{max}/V m^{-1})] and specific electrical capacitance of the SAIM (c/nF cm^{-2}). Other important characteristics of dielectric monolayers include the chemical nature of the end group, the density of defects and the crystal structure.

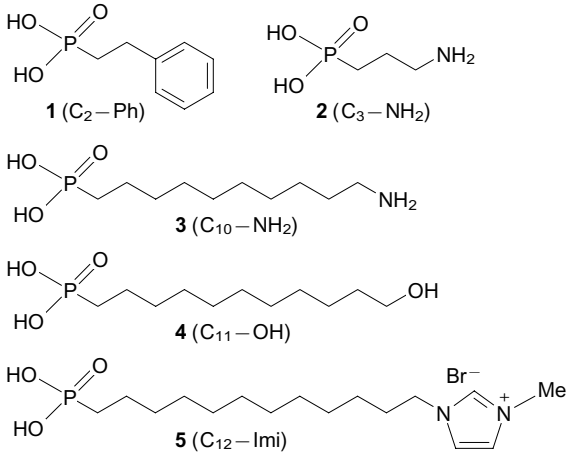
Pioneering studies on monolayer dielectric layers were intimately related to the design of molecular junctions. It was Vuillaume and co-workers[28] who proposed to utilize molecular junctions in OFETs in 2000. They used COOH-terminated n-alkyltrichlorosilane [$SiCl_3(CH_2)_{12}COOH$] as the SAIM precursor and α-sexithiophene as the OFET semiconductor layer. In spite of very small SAIM thickness (2.5 nm), the leakage current was reduced to $j = 10^{-6}$ A cm^{-2}. The OFET thus fabricated operated at low electrical voltages (< 2 V), which was a significant achievement for that time. A drawback of this approach consisted in interpenetration of the SAIM and organic semiconductor; this deteriorated the characteristics of the device.

To overcome this difficulty, Halik *et al.*[2] proposed to use an alkyltrichlorosilane with aromatic end group, *viz.*, (18-phenoxyoctadecyl)trichlorosilane, as precursor for the dielectric layer. Self-assembled interface layers based on this compound were 2.5 nm thick, which is slightly smaller than the calculated length of the molecule. Atomic force microscopy (AFM) and scanning tunnelling microscopy (CTM) studies of molecularly smooth SAIM revealed no defects. The layers were amorphous and the aromatic rings in individual molecules were randomly oriented. Contact angle (CA) measurements demonstrated an increase in the static CA from 10 to 95° upon SAIM formation and thus confirmed the formation of a dense hydrophobic layer. Noteworthy, the leakage current density was $j = (8 \pm 0.5) \times 10^{-7}$ A cm^{-2} and the breakdown field was $E_{max} = (14 \pm 2)$ MV cm^{-1}. These values are comparable or better than the corresponding values for silica,[29,30] which is traditionally used in complementary metal – oxide – semiconductor (CMOS) structures. Besides, the possibility to fabricate gold electrodes on SAIMs using photolithography and wet chemical etching was demonstrated and the possibility of utilizing SAIMs based on organosilicon dielectrics not only in nanoelectronics, but also in silicon CMOS technology was suggested. More recently, researchers from the group headed by Professor Halik extended the application field of these SAIMs to the fabrication of FETs based on carbon nanotubes.[31]

Yet another approach to high-quality monolayer dielectrics is to vary the nature of the anchor group to attain the highest SAIM density. Klauk *et al.*[20] proposed n-octadecylphosphonic acid (ODPA) and n-octadecyltrichlorosilane (ODTS) as precursors for the dielectric layer. Field-effect transistors were fabricated using glass or polyethylene naphthalate substrates coated with 20-nm Al layer deposited by thermal evaporation. The substrates with the aluminium layer were then plasma treated to form Al_2O_3 and create a high density of hydroxyl groups for subsequent formation of the SAIM through chemisorption. The monolayer dielectrics were studied by AFM, X-ray diffraction (XRD), X-ray photoelectron spectroscopy (XPS) and molecular modelling. It was shown that ODPA forms more dense SAIMs than ODTS on sapphire surface. Experiments with the ODPA SAIMs led to a very low leakage current of $(5 \pm 1) \times 10^{-8}$ A cm^{-2} at a voltage of 2 V. The ODPA monolayers were used to fabricate actually operating organic electronic devices, *viz.*, p- and n-type transistors and electronic circuits based on them.

Zaumseil and co-workers[32] studied the effect of the chemical structure of the self-assembled dielectric layer on the electrical properties of FETs based on single-walled carbon nanotubes (SWNTs) using organic phosphonic acid derivatives **1** – **5** as precursors. The phosphonic acid residue allowed one to grow SAIMs on alumina surface while different end groups made it possible to vary the surface properties. Single-walled

Structures 1 – 5



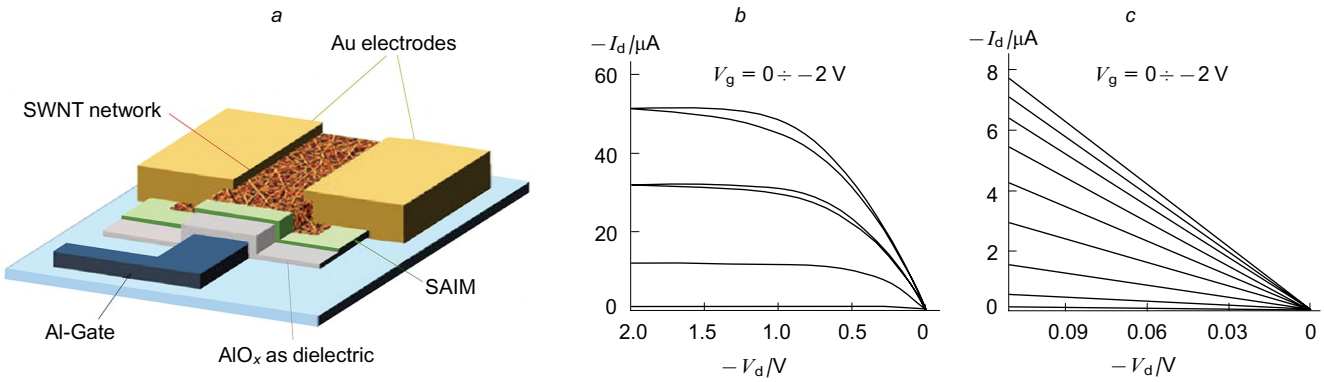


Figure 2. Schematic structure of field-effect transistor based on single-walled carbon nanotubes (*a*) and the output characteristics of the field-effect transistor with the dielectric layer containing hydroxyl end group (*b*, *c*).[32]
Notations: I_d is the drain current, V_d is the drain voltage and V_g is the gate voltage.

carbon nanotubes 0.9 – 1.9 nm in diameter were dispersed in poly(9,9-didodecylfluorene-2,7-diyl) and then spin coated (SCT) or solution deposited from toluene onto the SAIM surface, thus forming a semiconducting SWNT network. To study the electrical properties of the FETS in question, bottom-gate top-contact transistors (Fig. 2 *a*) were fabricated. Gold electrodes 30 nm thick were patterned on the semiconductor layer photolithographically.

It was shown[32] that the structure of the semiconducting network of solution-deposited SWNTs is determined by the structure of the SAIM grown on the alumina surface. The most dense semiconducting SWNT networks were prepared using the SAIMs with hydroxyl ($C_{11}-OH$) and imidazole ($C_{12}-Imi$) end groups. However, the FET operation efficiency was governed by not only the SWNT network density, but also the chemical structure of the dielectric layer. The best characteristics (on-conductance, low surface trap density, short critical channel length) were achieved for the devices with the dielectric monolayer containing hydroxyl end groups. The output curves for these FETs are presented in Fig. 2 *b*,*c*. The devices operated at low voltages (below 2 V) and demonstrated low hysteresis and low contact resistance, as can be seen in the linear characteristics at low voltages (see Fig. 2 *c*).

The possibility of spin coating the n-type semiconductor layer onto the ODPA SAIM was studied.[33] The authors developed an approach which is based on numerical analysis of the polar and dispersive contributions to the surface energy of solutions of organic semiconductors and allows one to predict the possibility of thin film formation on SAIm-modified sapphire. The approach proved itself for different organic compounds; the best OFETs were characterized by charge carrier mobilities in the range of 0.01 – 0.04 $cm^2\ V^{-1}\ s^{-1}$.

The alkyl chain length in the precursor molecule also significantly influences the dielectric properties of SAIMs.[34 – 37] For instance, a number of phosphonic acid derivatives with different alkyl chain length (C_2, C_6, C_{10}, C_{14} and C_{18}) were studied.[35] The electrical capacitance of the hybrid dielectrics based on SAIM-modified sapphire was measured by impedancemetry. In addition, the electrical capacitance of the SAIM grown on indium – tin oxide (ITO) was measured by cyclic voltammetry (CV), which eliminated the influence of dielectric properties of Al_2O_3. The electrical capacitance values measured by both methods were close and inversely proportional to the alkyl chain length. The SAIMs based on the same compounds were used to fabricate OFETs. The charge carrier mobility in the OFETs reached maximum values of 0.13 and 0.17 $cm^2\ V^{-1}\ cm^{-1}$ for C_{14} and C_{18}, respectively, and monotonically decreased with decreasing alkyl chain length. The effect observed was explained by disordering of short alkyl chains that deteriorated the morphology of the semiconductor layer.

The possibility of utilizing monolayer dielectrics for fabricating electronic devices based on individual SWNTs, *e.g.*, bottom-gate and top-gate FETs[38,39] with individual hydrothermally synthesized single-crystalline ZnO nanowire as the semiconductor[40] deserves attention. Efficient operation of the device was achieved by modifying the nanowire surface by the ODPA SAIM. Although the dielectric layer was only 2 nm thick, it provided efficient insulation of the semiconductor and gate. The schematic structures and transfer characteristics of the FETs based on individual nanowires the ODPA-modified dielectric layer are presented in Fig. 3. The addition of the dielectric layer significantly decreased the on and off currents. The calculated charge carrier mobility in the nanotube was 40 $cm^2\ V^{-1}\ s^{-1}$, the threshold voltage was about 0.5 V, while the on/off current ratio was 10^7. FET-based logic gates operating at frequencies below 1 MHz were also demonstrated and an important role of the SAIM in the attainment of high operating characteristics was pointed out.

The influence of the end group in the SAIM acting as the dielectric layer for an OFET on the properties of devices was studied systematically.[41 – 43] Examples are provided by OFETs based on two different organic semiconductors, pentacene and dihexylsexithiophene, and hybrid dielectrics composed of aluminium oxide AlO_x and SAIMs of different chemical structure.[41] The monolayer was formed using the following compounds: tetradecylphosphonic acid (SAIM1), a photosensitive material with C_{60} fullerene as the end group, [1-methoxy-3-(18-76 phosphonic acid octadecyloxy)methano]-1,2-dihydro[60]fullerene (SAIM2), and a mixture of SAIM1 and SAIM2 taken in a 99 : 1 mole ratio (SAIM3). The OFETs demonstrated photosensitivity; however, their properties depended strongly on the chemical structure of the SAIM. In particular, the elec-

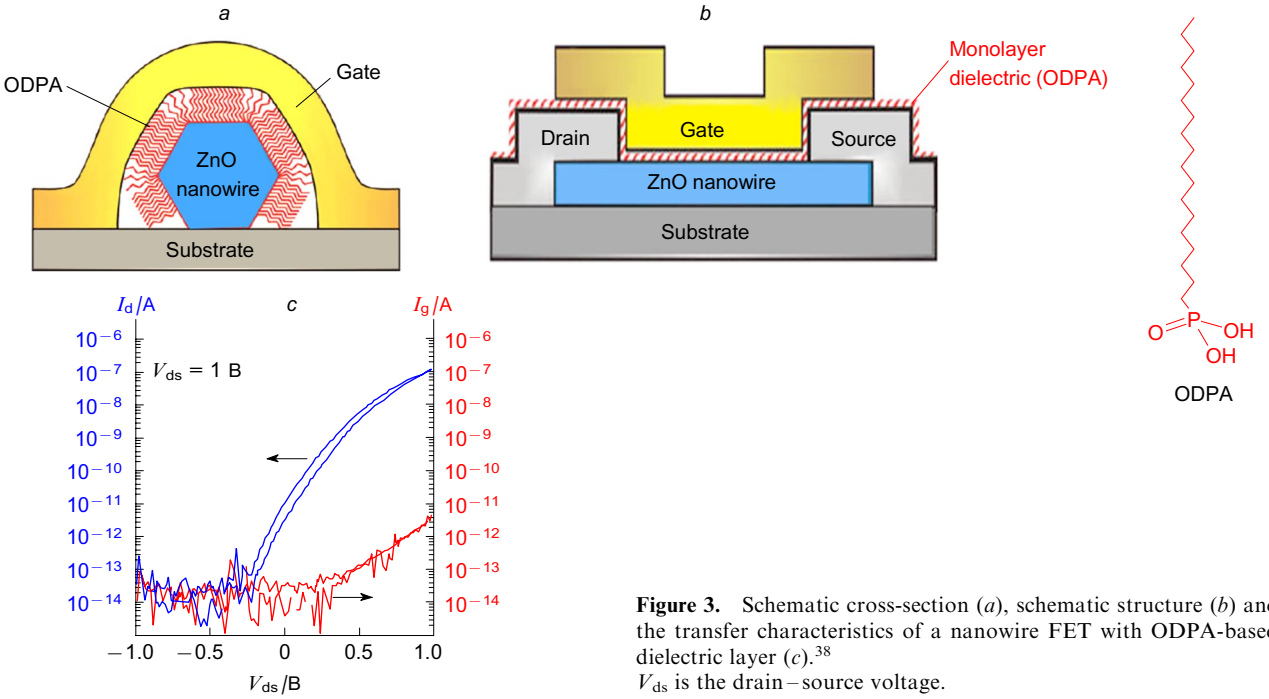


Figure 3. Schematic cross-section (*a*), schematic structure (*b*) and the transfer characteristics of a nanowire FET with ODPA-based dielectric layer (*c*).[38]
V_{ds} is the drain – source voltage.

trical properties of the OFET based on dihexylsexithiophene and SAIM1 and illuminated with monochromatic light at 658 nm (power intensity was 10 mW cm^{-2}) exactly matched those measured with no illumination. At the same time, doping SAIM3 with the photosensitive material (1%) led to a large shift of the transfer characteristic of the transistor under illumination with monochromatic light at 658 nm. The effect observed was explained by photoexcitation of charges at the dielectric/semiconductor interface. At the same time, no photoexcitation was observed using SAIM2 and the same semiconductor. This was explained by the carrier density saturation at the semiconductor/dielectric interface even in the absence of external illumination. Based on the results obtained, it was concluded that the chemical structure of SAIM as the component of the hybrid dielectric has strong effect on the optical properties of the OFETs.

Heteroatoms as constituents of aliphatic spacer in the precursor also significantly influence the properties of SAIMs.[44,45] In particular, SAIMs based on 2-[2-(2-methoxyethoxy)ethoxy]ethylphosphonic acid [$CH_3(OC_2H_4)_3$-PA] containing an oligo(ethylene glycol) chain and doped with various salts [LiCl, NaCl, KCl, NH_4Cl, $N(CH_3)_4Cl$] were studied by molecular dynamics and molecular modelling.[44] The results of modelling correctly predict the SAIM affinities to various cations while the electrical properties of FETs fabricated using ion-doped SAIMs were significantly different for different ions. An important practical consequence of that study was a threefold increase in the charge carrier mobility in the FETs and a decrease in the threshold voltage. It was concluded that ion doping of SAIMs is a simple and promising technique for FET applications.

Recently, hybrid dielectrics comprising dielectric films with high dielectric constant (so-called high-k-dielectrics) and SAIMs have been intensively studied.[46–49] Interest in these systems is due to the possibility to increase the specific electrical capacitance of the FET dielectric and thus increase the charge carrier density in the FET channel at low voltages. For instance, self-assembled hybrid nanodielectrics representing periodic structures comprised of pairs of oxide (HfO_x, ZrO_x and SiO_x) thin films and SAIMs (Fig. 4) were reported.[47] π-Conjugated phosphonic acid derivatives (see right part in Fig. 4 *b*) were utilized as SAIM precursors. Multilayer hybrid nanodielectrics were studied by XRD and simulated within the framework of the density functional theory. It was shown that, irrespective of the precursor type, the axes of the conjugated molecules are oriented normal to the surface where self-assembly of the SAIM occurs. At the same time, the chemical structure of the SAIM precursor determines the FET threshold voltage. Taking account of extremely high specific electrical capacitance (400 – 1000 nF cm^{-2}), such hybrid nanodielectrics are promising for practical applications in organic and hybrid electronic devices.

Hybrid inorganic/organic structures were tailored[50] using a FET dielectric representing alternating layers of alumina and organic phosphonic acid derivatives (Fig. 5 *a*). The approach enabled significant enhancement of charge carrier mobility in the FETs and improvement of the FET stability. There exists a threshold dielectric surface roughness such that additional hybrid dielectric layers improve the electrical properties of the FET at smaller roughness values and deteriorate them otherwise.

The charge carrier mobility is plotted *vs.* number of hybrid dielectric layers for three phosphonic acid (PA) derivatives in Fig. 5 *b*. In the case of monolayer hybrid dielectrics the chemical structure of the monolayer (alkyl chain length) had little effect on the OFET properties. As the number of the SAIM/Al_2O_3 hybrid dielectric layers increased, the alkyl chain length influenced the charge carrier mobility in different manner. In particular, for the

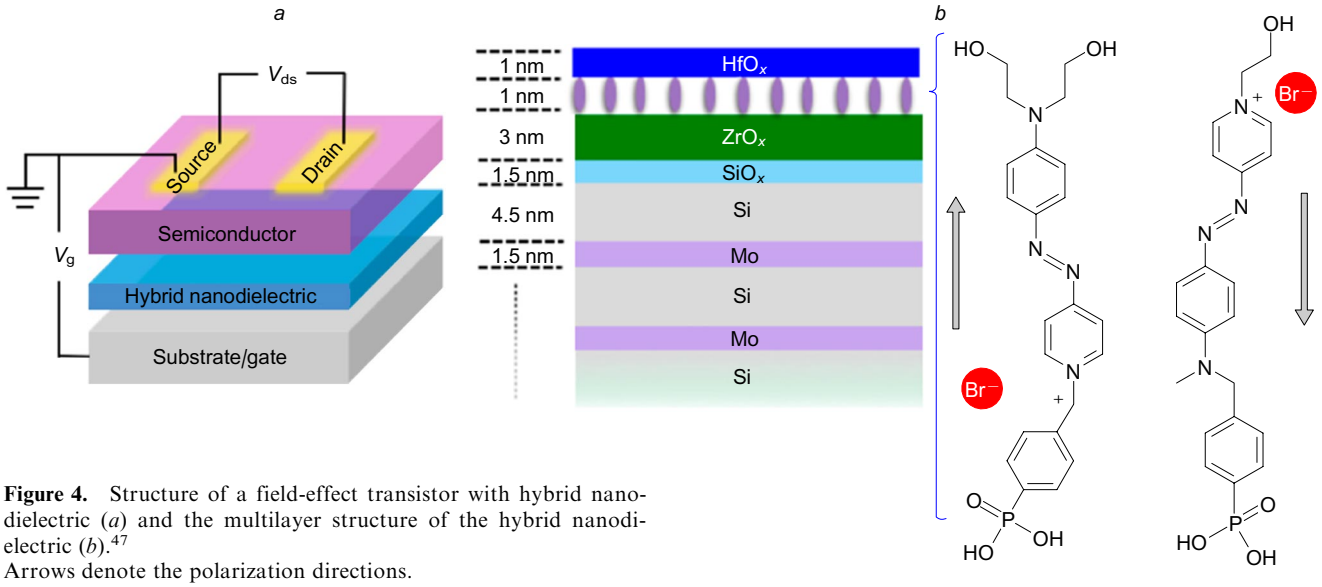


Figure 4. Structure of a field-effect transistor with hybrid nanodielectric (*a*) and the multilayer structure of the hybrid nanodielectric (*b*).[47]
Arrows denote the polarization directions.

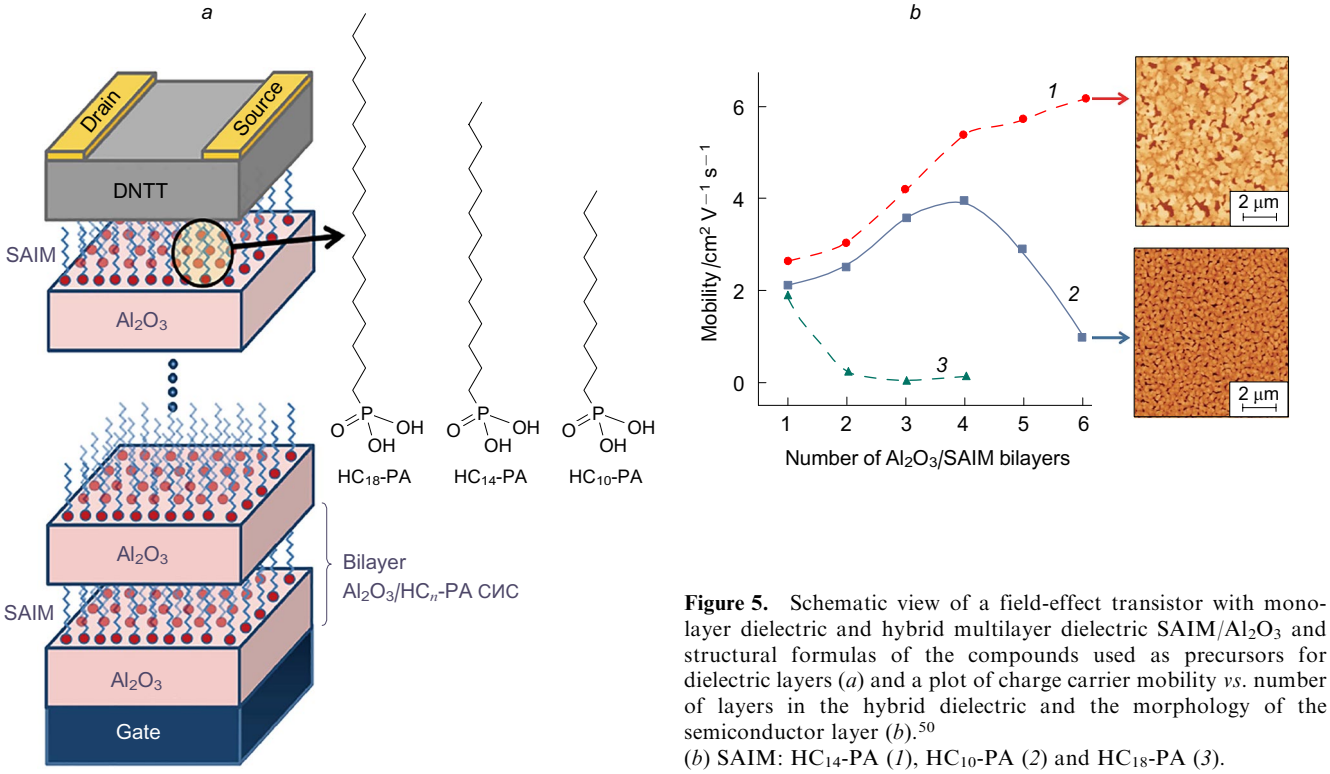


Figure 5. Schematic view of a field-effect transistor with monolayer dielectric and hybrid multilayer dielectric SAIM/Al_2O_3 and structural formulas of the compounds used as precursors for dielectric layers (*a*) and a plot of charge carrier mobility *vs.* number of layers in the hybrid dielectric and the morphology of the semiconductor layer (*b*).[50]
(*b*) SAIM: HC_{14}-PA (*1*), HC_{10}-PA (*2*) and HC_{18}-PA (*3*).

long chain C_{18} the charge carrier mobility in the OFET abruptly decreased even when two dielectric layers were used. This effect was explained by high roughness of the SAIM surface when the second layer was applied. At the same time, the maximum charge carrier mobility for the C_{10} chain was observed at four hybrid dielectric layers, which corresponded to the largest area of the semiconductor domain. The effect was also associated with the optimum roughness of the dielectric surface (5 nm). Eventually, combining the dielectric layer with the C_{14} alkyl chain and dinaphtho[2,3-*b*:2′,3′-*f*]thieno[3,2-*b*]thiophene (DNTT) as the semiconductor led to a maximum charge carrier mobility of 6 $cm^2\ V^{-1}\ s^{-1}$. This result indicates that hybrid dielectric layers SAIM/Al_2O_3 are promising for fabrication of organic electronic devices.

Concluding this Section, it should be noted that the development and fabrication of SAIMs for monolayer and hybrid dielectrics is a topical line of scientific research. The data presented above show that the number of publications on this subject has continuously increased in the last decade; however, the focus of research varies from one year to another. For instance, the most important avenue of recent research involves fabrication of hybrid multilayer SAIM-modified dielectrics. This offers

prospects for fine tuning the surface and dielectric properties of the films, which in turn enables significant improvement of characteristics of FETs that are basic functional units of microelectronic devices.

3. Self-assembled interface layers as adhesion promoters

Among various applications of SAIMs in organic and hybrid electronics, the design of SAIM-based promoters of adhesion between conductive structures and chemically inert surface of polymeric substrates deserves particular attention.[9,10] This is a topical problem for, *e.g.*, manufacturing of flexible circuits where conductive paths are basic units and therefore relevant methods for their fabrication by inkjet printing or spraying are needed.

One of the first studies on fabrication of organic interface layers as adhesion enhancers for microelectronic devices was reported by researchers working at IBM Corp. (USA).[51] A self-assembled layer based on (3-mercaptopropyl)trimethoxysilane (MPTS) was used to enhance copper adhesion to silica and to suppress copper diffusion into the bulk of SiO_2. More recently it was shown that MPTS can also be used in the case of polymeric substrates.[52] A SAIM was fabricated[51] by ozone plasma treatment of SiO_2 followed by immersion in MPTS solution (5 mmol litre^{-1}). The presence of the interface layer was proved by ellipsometry and high-resolution XPS. Then, the interface layer was coated by chemical vapour deposited copper. Mechanical properties of the Cu/SAIM/SiO_2 and Cu/SiO_2 samples were studied by analyzing the load – displacement plots. It was found that the debond energy increased from 3.1 for Cu/SiO_2 to 9.2 J m^{-2} for Cu/SAIM/SiO_2. In addition, the leakage currents were studied as function of annealing time. These dependences are indicative of coper diffusion into the bulk of SiO_2. It was shown that the addition of the MPTS layer suppresses of copper diffusion. This result is of great practical importance for production of microelectronic devices.

Selective metallization of polymeric substrates using an interface layer based on PEI, PAA and a platinum catalyst was reported.[53] The process is schematically shown in Fig. 6. In the first step the substrate based on PET, PEN or PI was cleaned in acetone and then γ-irradiated to produce surface radicals (see Fig. 6 *a*). Next, substrates were placed in acrylic acid solution where surface polymerization resulting in PAA grafted to the substrate (see Fig. 6 *b*) was carried out in nitrogen stream at 80 °C for 2 h. In the third step, the modified surface was patterned by screen printing using a chemically inert mask. The substrate with the mask was immersed into 10% aqueous PEI solution (see Fig. 6 *c*). In the final step the substrate was immersed into a solution containing $PdCl_2$. The palladium catalyst was then activated and copper circuit patterns were fabricated in the Pd-containing regions on the substrate surface by immersing into electroless Cu solution (see Fig. 6 *d*). The interface layers and circuit patterns based on them were characterized by IR spectroscopy, by CA measurements, XPS and transmission electron microscopy. The adhesion between the copper inks and the substrate was measured using a standard peel adhesion test (ASTM D3359B-02). It was concluded that the

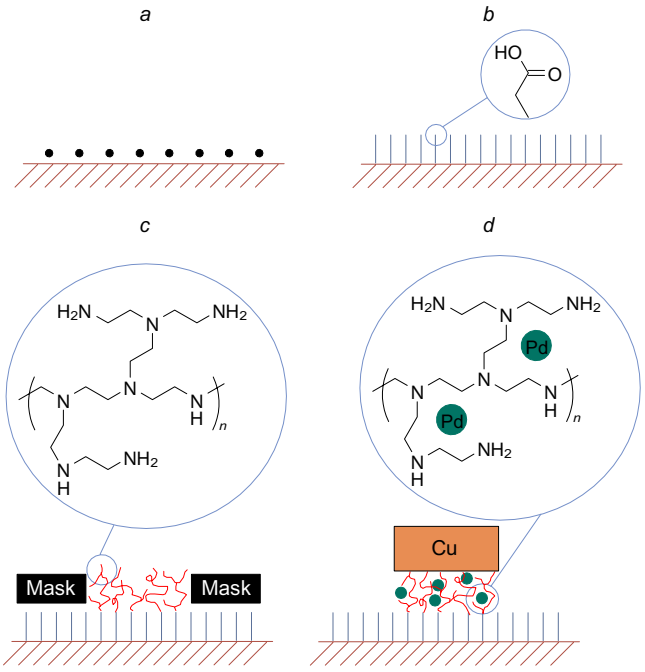


Figure 6. Fabrication of conductive copper structures on a polymeric substrate: a schematic.[53]
Surface modification using adhesive interface layer based on PEI, PAA and platinum catalyst (including cleaning of the substrate followed by γ-irradiation) (*a*); surface polymerization in acrylic acid solution (*b*); patterning the modified surface using a chemically inert mask (*c*); and storage of the substrate in a solution containing $PdCl_2$ as catalyst (*d*).

method proposed is universal and has a great potential for practical applications owing to high mechanical strength of the final structures and to the possibility of using printing techniques for modification of polymers.

Yet another method for deposition of conductive coatings is to use two types of SAIMs, 6-(3-triethoxysilylpropylamino)-1,3,5-triazine-2,4-diazide (P-TES) and 6-(3-triethoxysilylpropylamino)-1,3,5-triazine-2,4-dithiolate monosodium (N-TES).[54–56] This approach can be exemplified by the study by Chen *et al.*,[55] who proposed layer-by-layer coating of a polymer surface with silver inks to attain high adhesion of conductive silver patterns to the substrate based on acrylonitrile butadiene styrene (ABS plastic). The process is schematically shown in Fig. 7. In the first step the polymer was modified by the P-TES SAIM by immersion in a P-TES ethanol solution (2 mmol litre^{-1}) followed by UV irradiation and sonication. The modified substrates were immersed in N-TES aqueous solution (2 mmol litre^{-1}) for 10 min at 70 °C. As a result of condensation reaction, a common SAIM with surface thiol groups formed on the polymer surface. This allowed one to expect high adhesion between the substrate and silver film. Silver conductive films are formed by the silver mirror reaction which involves reduction of silver in Tollens' reagent. The addition of a reducing agent containing glyoxal was followed by the formation of metallic silver. Tollens' reagent and the reducing agent were successively sprayed onto the surface;[55] the number of spraying cycles for each component was varied to fabricate the optimum coating.

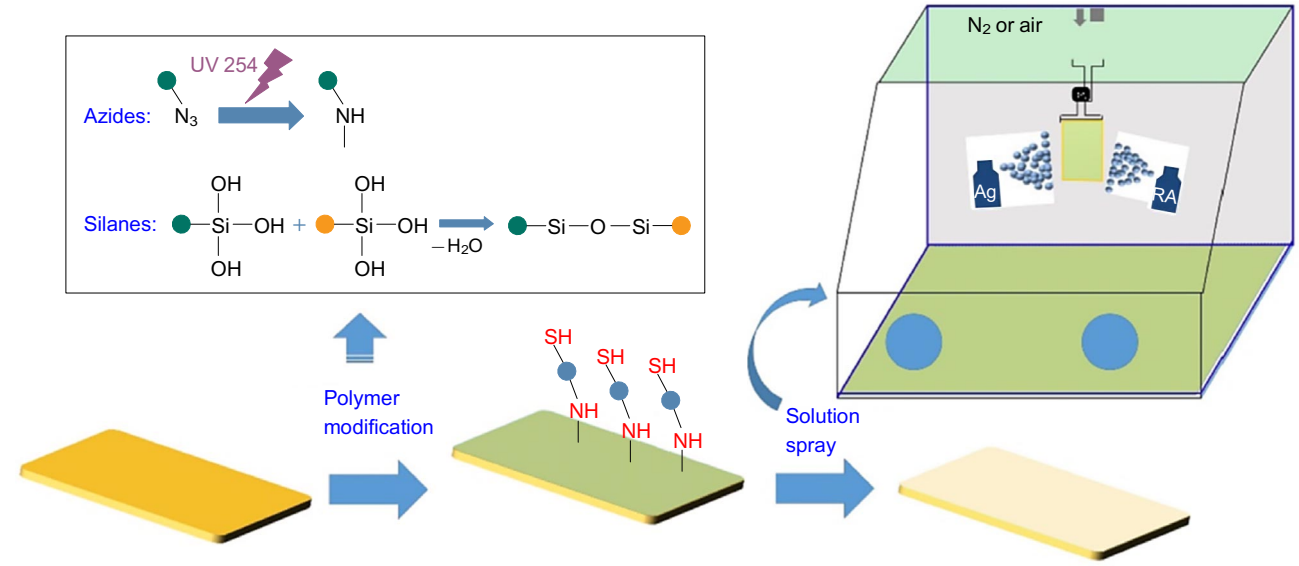


Figure 7. Modification of ABS substrate using self-assembled interface layers and fabrication of Ag-based conductive structures by spray printing using two solutions.[55]

Studies of the SAIMs thus fabricated made it possible to establish mechanisms of nucleation and subsequent growth of silver nanoparticles formed upon spraying. Optimum fabrication conditions were chosen to improve the mechanical strength of conductive coatings. The results of XRD, XPS and angle-resolved XPS studies showed the presence of a small amount of silver oxide that was mainly localized in the near-surface layer. It was found that the coating is covalently bound to the substrate, which provides high adhesion to the ABS plastic. Unfortunately, no electrical properties of the silver films were reported; however, taking account of the method used for fabrication of the silver coating allows one to assume that they were not good. Other drawbacks of this approach include the use of two reactive compounds and the impossibility to carry out local modification.

It was proposed to improve the printing quality of conductive silver nanoinks on chemically inert polymer surface and the adhesion between the conductive layer to the substrate using SAIMs.[21,52] The modifiers chosen were MPTS, (3-aminopropyl)trimethoxysilane (APTS) and oligo[(3-mercaptopropyl)(methoxy)siloxane] (OMPMS). Methoxysilyl functional groups allowed these compounds to form covalent bonds with hydroxyl groups on the surface of the plasma-pretreated polymer. In addition, the three compounds contained thiol or amino groups able to form covalent or coordination bonds with silver atoms. The polymeric substrates were PEN and polydimethylsiloxane (PDMS).

Polymer surface modification by organosilicon materials APTS/MPTS/OMPMS is schematically shown in Fig. 8.[21,52] First, the chemically inert polymer was treated in oxygen plasma to provide formation of surface hydroxyl groups. Then, the polymer was coated by adhesion promoter layers using vapour phase deposition, spin coating technique or inkjet printing to form a self-assembled multilayer structure through the interaction of siloxane groups with one another and with the surface hydroxyl groups. The modification using vapour phase deposition was carried out using highly volatile low-molecular-mass agents APTS and MPTS. The other two techniques, SCT and inkjet printing, imply liquid-phase modification using oligomeric OMPMS. They are suitable for practical applications including local modification.

The self-assembled adhesive organosilicon layers were studied by AFM, XPS and CA measurements. The morphologies of the PDMS film before and after vapour-phase deposition of MPTS and spin coating of OMPMS are presented in Fig. 9 *a*–*c*. An analysis of the morphology at different regions of the substrates confirmed high homogeneity of the modified polymer surface. The formation of interface layer on the surface was suggested based on significant morphological differences between the bare and modified PDMS. The layer thickness could not be reliably determined by AFM owing to high surface roughness of the bare substrate. The maximum height difference for the bare substrate was more than 1.2 μm (*cf.* 200 and 500 nm for the MPTS- and OMPMS-modified surfaces, respectively, see Fig. 9 *d*–*f*). This result, explained by pore filling in the bare PDMS during the SAIM formation, was an extra benefit from the modification with adhesion promoter, since more smooth substrate surface should potentially improve its properties as precursor for printed electronic devices.

An analysis of the XPS spectra of the bare and modified polymeric substrates PEN and PDMS also proved the formation of SAIMs on the polymer surface. Contact angle measurements confirmed successful modification of the substrate surface using PDMS. The bare polymer is a hydrophobic material characterized by CA = 118 ± 5°. Plasma treatment imparts superhydrophilic properties to the substrate (CA ~ 0°) while modification by adhesion promoter causes CA to increase. It

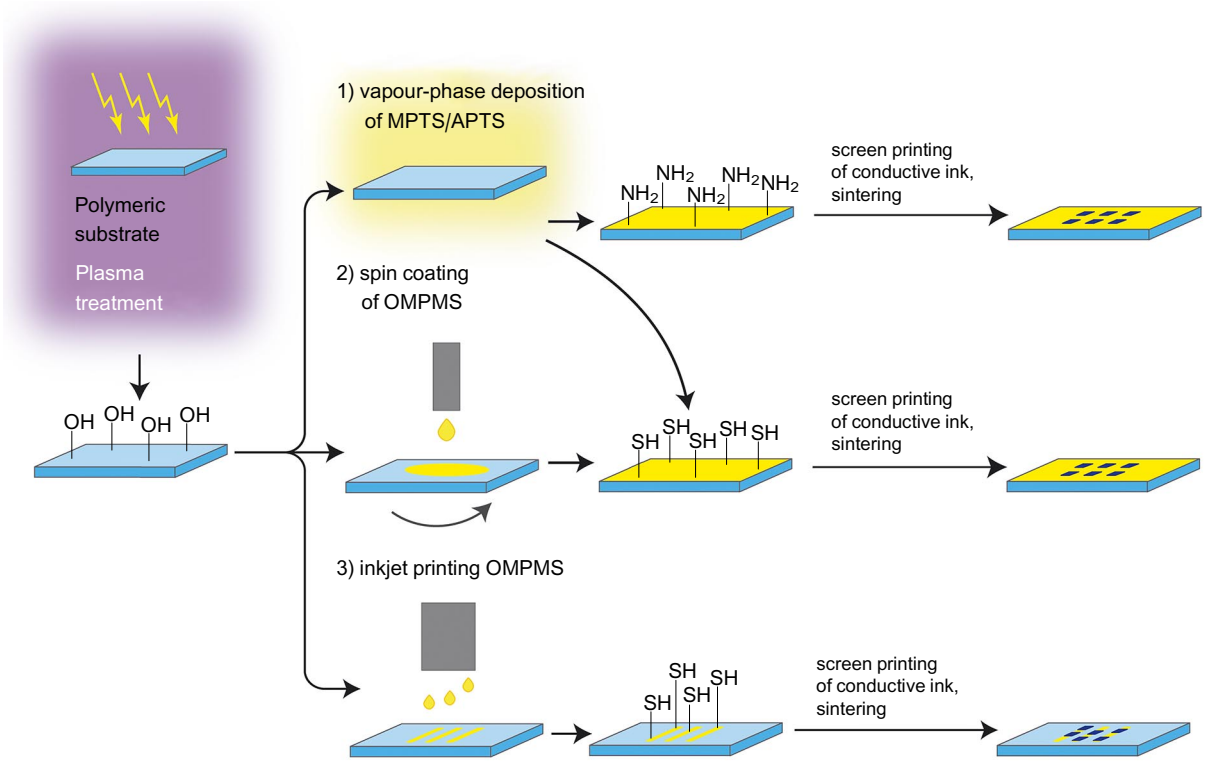


Figure 8. Polymer surface modification by adhesion promoters APTS/MPTS/OMPMS: a schematic.[21, 52]

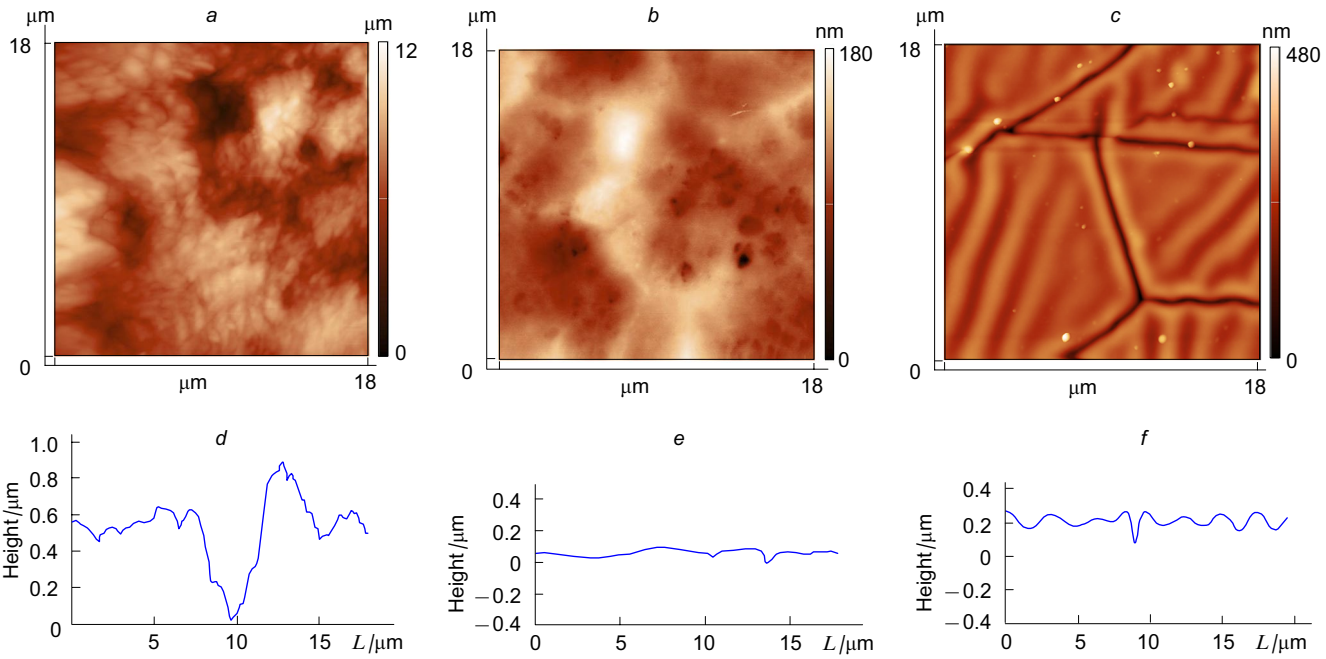


Figure 9. The AFM morphology of PDMS before (*a*) and after (*b*) vapour-phase deposition of MPTS, and after spin coating of OMPMS (*c*); and the corresponding AFM surface profiles (*d*–*f*).[21, 52]

was found that for vapour-phase deposition of MPTS the CA depends on the deposition time, being equal to $107 \pm 3^\circ$ for 2 h and to $99 \pm 3^\circ$ for 72 h of treatment. This dependence was explained by an increase in the average thickness of the SAIM containing both hydrophobic siloxane and hydrophilic amino groups and by a decrease in the roughness of the polymer surface.

Adhesion evaluation results for conductive structures based on aqueous and organic silver nanoinks to the PDMS substrate modified by different vapour-phase

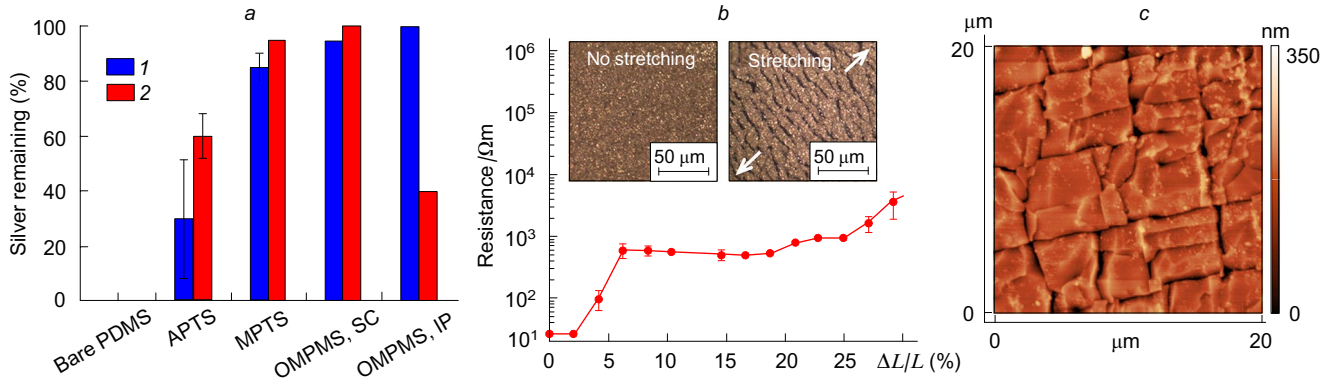


Figure 10. Adhesion evaluation results for Ag inks to PDMS using the crosshatch tape test for different adhesion promoters and deposition techniques (*a*), resistance of silver conductive inks plotted *vs.* relative elongation of MPTS-modified PDMS substrate (*b*), and the morphology of silver inks upon stretching (*c*).[21,52]
(*a*) Aqueous inks (*1*) and organic-based inks (*2*).

deposited and spin coated adhesion promoters using the crosshatch tape test are shown in Fig. 10. Bare PDMS is characterized by zero adhesion to both types of inks, whereas vapour-phase deposition and spin coating led to 90% and 100% adhesion, respectively. The effect of thiol-containing promoters on adhesion of Ag inks is stronger than that of amino-containing promoters. This can be explained by higher affinity of silver to thiol groups compared to amino ones owing to formation of strong covalent bonds in the former case and complexation in the latter.

Figure 10 *b* presents the dependence of the resistance of silver conductive structures printed on the MPTS-modified PDMS substrate on the relative elongation of the polymer ($\Delta L/L$) . The inks retain conductive properties up to a relative elongation of 30%. At the same time, stretching of the substrate is accompanied by intense cracking of the conductive film (see Fig. 10 *c*) and thus considerable increase in the total resistance. Nevertheless, the inks demonstrated high adhesion to the substrate and withstood 1000 stretching–compression cycles without visible delamination. Therefore, the interface layers thus fabricated can be used in organic electronic chips operating under moderate stretching loads.

Concluding this Section, it should be noted that changes in the surface properties of substrates including adhesion improvement of conductive structures using SAIMs is a topical avenue of applied research. In some cases SAIMs allow one to attain 100% adhesion of conductive structures to chemically inert polymeric substrates.

4. Self-assembled interface monolayers for nanostructured surface formation

Most studies on SAIMs for organic and hybrid electronics are aimed at fabricating highly homogeneous interface layers with nearly 100% coverages and smallest surface roughness. Besides, of particular interest are studies focused on the formation of nanostructured surfaces using SAIMs since such surfaces have a great potential for practical applications. Main methods for fabrication of SIAM-nanostructured surfaces include microcontact printing,[57,58] photolithography[59,60] and various versions of these techniques. The most interesting relevant examples will be considered in this Section.

A method proposed[57] for controlling the local efficiency of OLED luminescence using nanostructured SAIMs is based on a strong correlation between the luminescence efficiency and the electrode work function difference (ΔW). Structure modification using SAIMs allows one to vary ΔW and, as a consequence, the charge carrier density in the active layer. If the surface of an electrode is structured using a SAIM, the local luminescence efficiency depends on the SAIM properties at a given point.

Structured SAIMs were prepared by microcontact printing using a stamp based on structured PDMS. The stamps were placed in a 2 mM solution of octadecane-1-thiol ($C_{18}H_{37}SH$) or 13,13,14,14,15,15,16,16,16-nonafluorohexadecane-1-thiol ($C_4F_9C_{12}H_{24}SH$) for 1 h. Both compounds were chosen based on the assumption that SAIMs based on them have oppositely oriented dipole moments so one could expect opposite effects on the luminescence efficiency. Then, the stamp was rinsed in ethanol and dried in nitrogen stream. In the final step, the stamps soaked with the solvent were pressed onto an Au surface to pattern a SAIM of $C_{18}H_{37}SH$ or $C_4F_9C_{12}H_{24}SH$. The SAIMs thus prepared were studied by AFM, scanning Kelvin probe microscopy (SKPM), polarized light microscopy; their OLED properties were also assessed. It was shown that the proposed method for local modification of luminescence efficiency is operative and that the lateral resolution for work function modification is less than 100 nm.

Yet another approach to formation of nanostructured surfaces is based on photolithography. For instance, modification of multifunctional surfaces containing different reactive groups (amino, thiol, methyl, carboxyl and fluoro) on the same structured substrate was reported.[61] The order of operations is as follows:

— growth of ODTS monolayer on silica surface;

— UV-ozone patterning of the monolayer using a photomask (Fig. 11);

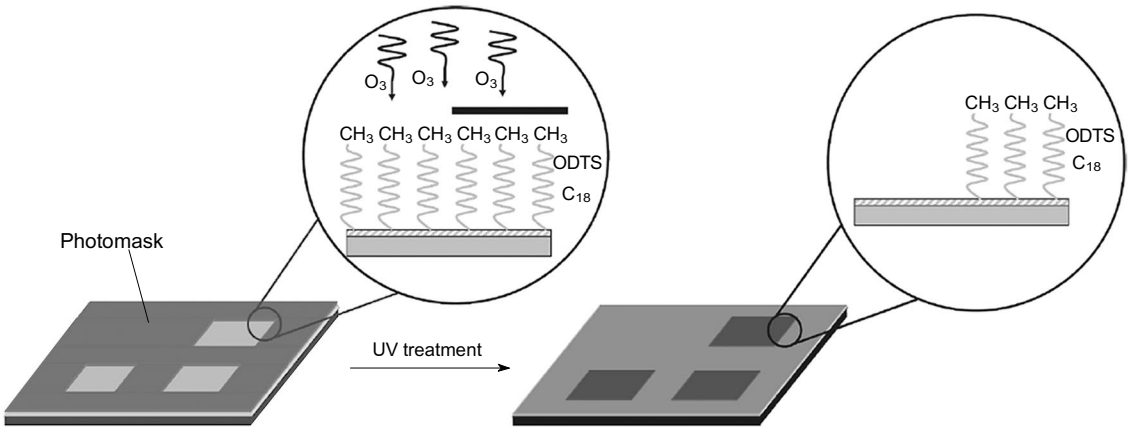


Figure 11. Patterning of ODTS SAIM for subsequent formation of nanostructured surfaces: a scheme.[61]

— coating of the patterned areas with SAIMs of other trichlorosilanes (*e.g.*, 11-bromoundecyltrichlorosilane, perfluorodecyltrichlorosilane); and

— surface modification of bromine-containing areas of the monolayer into amine- and thiol-terminated regions or electro-oxidative lithography involving conversion into carboxyl end groups.

The modified surfaces were characterized by CA measurements, IR spectroscopy and AFM. In addition, the interaction of the modified substrate surface regions with Si and Au nanoparticles and with hydroxyl-functionalized micelles was analyzed. It was shown that the method proposed enables local self-assembly of different nanoparticles on specified regions of the modified substrate, which can be promising for, *e.g.*, the design of biosensors and bioassay.

An international group of researchers from India, Israel, the Netherlands, and China compared solution-phase and wetting-driven monolayer self-assembly taking linear carbosilanes as examples.[62] It was reported that SAIMs are formed owing to hydrophobic properties of the precursor compounds containing long aliphatic fragments that facilitate direct visualization of the self-assembly without using sophisticated analytical equipment.[63] Hydrophobic character of the SAIMs makes it possible to precisely control the self-assembly of discrete, well-defined monolayers, while alternation of hydrophobicity and hydrophilicity in systems of bifunctional carbosilanes allow one to practically implement self-assembly of multilayer materials.[64, 65] The possibility to fabricate templates based on SAIMs with hydrophobic and hydrophilic properties at preset confined areas was reported.[66] Both highly ordered monolayers based on linear carbosilanes and thicker layer-by-layer assembled structures are suitable for creating templates. Agarose and eicosene functional derivatives were used to demonstrate the potential of the new versions of self-assembly techniques, namely:

— wetting-driven controlled deposition on hydrophobic-hydrophilic monolayer and bilayer templates at elevated temperatures;

— melt and solution deposition involving solidification at ambient temperature; and

— possible extension of constructive nanolithography to thicker layer-by-layer grown films, which offers prospects for 3D organization of templates based on monofunctional n-alkylsilanes.

A critical assessment of application fields, advantages and limitations of various methods for bottom-up fabrication of surface structures of different length scales (from nano- to macroscale) was reported.[67]

Structured SAIMs can be prepared by microcontact printing[68] using a paraffin stamp fabricated by 3D-printing. The SAIM precursors were organosilicon derivatives (*e.g.*, ODTS), phosphonic acid derivatives (*e.g.*, ODPA) and thiols (dodecane-1-thiol). The microcontact printing process is schematically shown in Fig. 12. A stamp of specified shape was made of molten paraffin and place in a precursor solution. Since the compounds under study were diphilic, keeping the stamp in solution was accompanied by self-assembly of SAIM through the interaction between paraffin and the hydrophobic fragments of the material. Structures thus fabricated were studied by AFM, XRD and CA measurements and IR

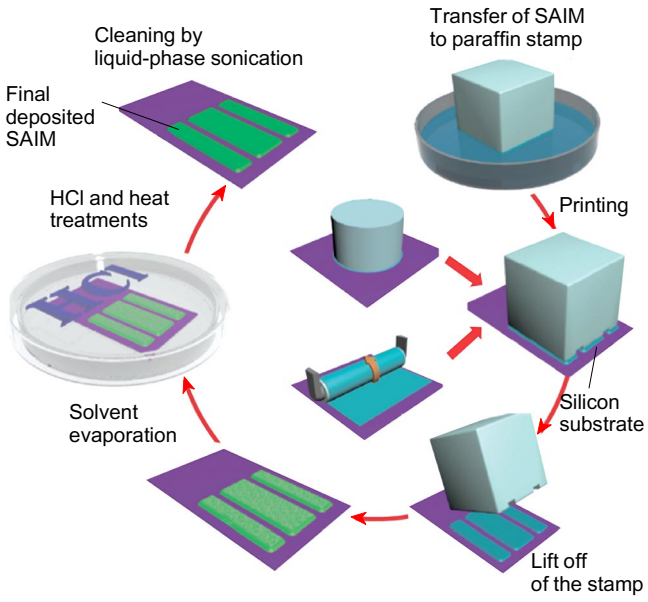


Figure 12. Formation of structured SAIM surface by microcontact printing: a schematic.[68]

spectroscopy. It was shown that the SAIMs are macroscopically homogeneous and characterized by high packing density. Dielectrics with structured surface were used to fabricate organic electronic devices like OFETs and inverters based on them. It was concluded that this patterning technique is universal and can be used for mass production of dielectrics.

Of particular interest is a study[69] on microcontact printing of two-composite surface using two different molecular inks (*e.g.*, bovine serum albumin and polyethylene glycol). The method involves four steps, namely, (i) microcontact printing of type-1 inks, (ii) degassing of the PDMS-based stamp to remove the air, (iii) patterning of the free surface of the stamp using type-2 inks; and (iv) removal of the stamp to get a micropatterned array of functional molecules on the substrate. The advantage of this technique consists in the possibility of microcontact printing using different inks without replacement of the stamp and its orientation on the substrate. The process can be widely used in biomedical applications.

In conclusion, mention should be made that the total number of yearly published studies on nanostructuring of surfaces using SAIMs is small owing to limited set of known patterning techniques and technical character of results obtained. At the same time, the importance of this application of SAIMs and a great potential of surface nanopatterning for practical applications are undoubtful.

5. Self-assembled interface monolayers at semiconductor/dielectric interface in field-effect transistors

As mentioned above (see Introduction), hybrid electronics often requires that organic semiconductor materials be combined with silicon and silica. This can be done using SAIMs. The authors of a key study on interface layers in FETs[22] used a SAIM fabricated by vapour-phase deposition of hexamethyldisilazane (HMDS) on 10-min pre-ozonated silica surface. Prior to depositing SAIM, gold drain and source electrodes (channel width was 2500 μm and channel length was 10 μm) were patterned on Si wafers by photolithography. In the experiments, the coverage of silica with HMDS was controlled by varying the time of the vapour exposure. The organic semiconductor for the OFET was poly-TAA with a charge carrier mobility of $10^{-3}-10^{-2}$ cm^2 V^{-1} s^{-1}. Schematic cross-section of the device and the chemical formula of the semiconductor used are presented in the inset in Fig. 13 *a*.

A study[22] on stability of electrical characteristics of OFETs revealed gradual degradation of the device having no interface layer fabricated by treatment with HMDS. Namely, the transfer characteristics shifted towards negative voltages (see Fig. 13 *a*). This effect was explained by the presence of charge carrier traps on the silica surface. Application of a nonzero external voltage was followed by charge injection from electrodes into the semiconductor layer while charge trapping on the dielectric surface led to shift of the threshold voltage. The OFET threshold voltage is plotted *vs.* time in Fig. 13 *b*. Based on the assumption of appearance of carrier traps, a theoretical description of the process was proposed and the following equation relating the threshold voltage to time was derived:

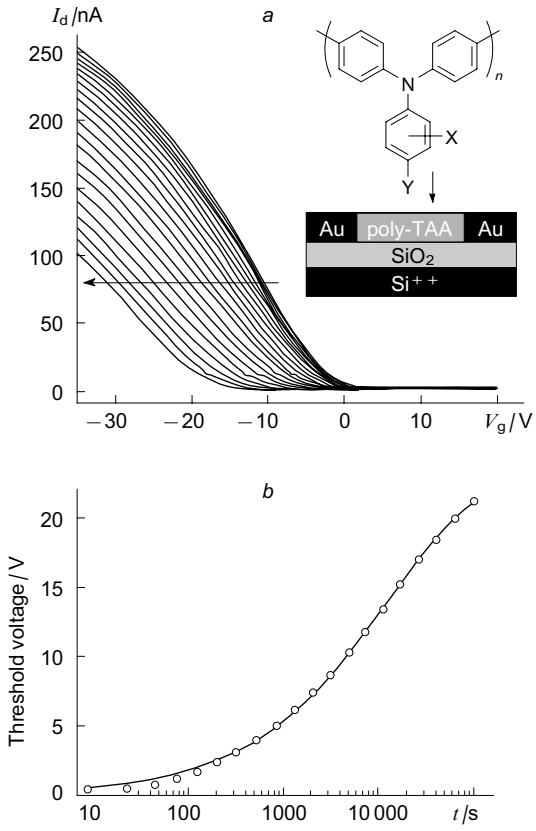


Figure 13. Transfer characteristics of an OFET with no interface layer measured at constant voltages during 27 h of continuous tests (*a*) and the OFET threshold voltage plotted *vs.* time (*b*).[22]
X and Y are short-chain alkyl substituents.

$$\Delta V_t = 1-\exp\left[-\left(\frac{t}{\tau}\right)^{\beta}\right] \quad (1)$$

where ΔV_t is the change in the threshold voltage as function of time, τ is the time constant, β is the dispersion parameter related to temperature as $\beta = T/T_0$ (the T_0 value was determined from the spectral width of the density of states for charge traps). Experimental data (see Fig. 13 *b*) were correctly approximated using Eqn (1) at τ = 1000 s and β = 0.5.

It was found that deposition of HMDS-based SAIM significantly suppressed trapping and, as a consequence, reduced degradation of the OFET with time. The local potential distribution on the dielectric surface between the drain and source electrodes of the transistor on SiO_2 substrate with HMDS interface monolayer (no semiconductor layer) at different coverages with HMDS (SKPM data) is presented in Fig. 14. The curves were successively recorded with 6 s time intervals, the potential of the drain electrode was maintained at 10 V, while the source and gate electrodes were connected to ground. An abrupt local potential drop was observed at a HMDS coverage of 53% (see Fig. 14 *a*) and persisted in time. As the coverage of silica surface with the interface layer decreased, the potential gradually smeared with time (see Fig. 14 *b*,*c*). This effect was explained by trapping charge carriers on the surface of bare SiO_2. No hydroxyl

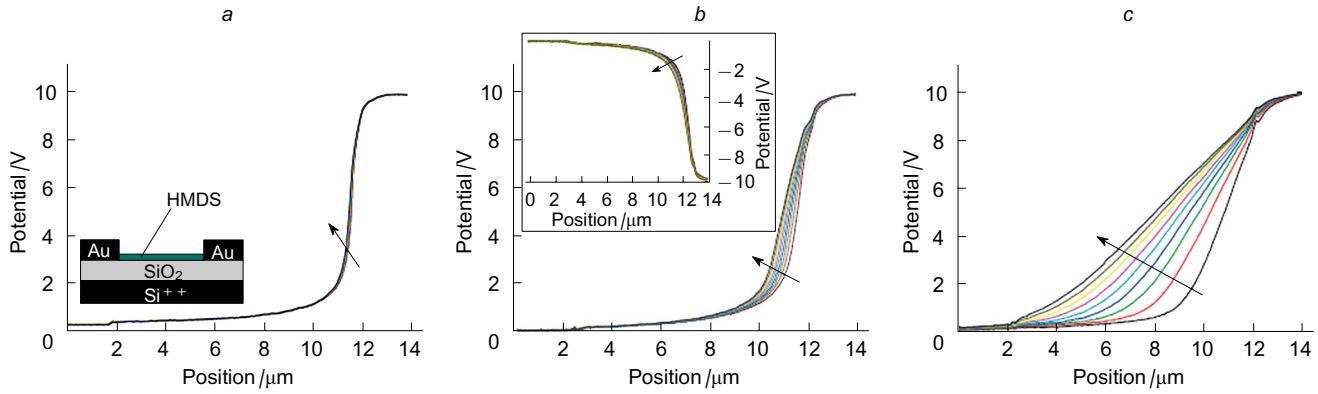


Figure 14. Local potential distributions on the dielectric surface between the drain and source electrodes of a transistor on SiO_2 substrates with HMDS-based interface layer (no semiconductor layer) at a HMDS coverage of 53 (*a*), 42 (*b*), and 14% (*c*).[22] Arrows denote the sequence of measurements.

groups are present on the surface of HMDS-treated substrate and the potential is not smeared. To prove this hypothesis, the coefficient β was calculated for the 'no semiconductor' case. Its value appeared to be equal to that determined from the dependence of the threshold voltage on time (see Fig. 13 *b*), thus indicating an identical nature of these phenomena. It was concluded that it is the surface traps that are responsible for the shift of the threshold voltage. Treatment with HMDS allows one to suppress this process.

The influence of the SAIM chemical structure on the threshold voltage was studied[70] taking OFETS with conventional architecture as examples; the SAIM chemical structure was varied using different end groups. Three triethoxysilanes studied were $CF_3(CF_2)_7(CH_2)_2Si(OC_2H_5)_3$, $CH_3(CH_2)_9Si(OC_2H_5)_3$ and $NH_2(CH_2)_3Si(OC_2H_5)_3$. According to XRD and AFM data and the results of CA measurements, all of them formed SAIMs on silica surface. The SAIM thickness determined from X-ray scattering data corresponded to the calculated length of the molecules. It was established that SAIMs significantly change the OFET threshold voltage, *viz.*, the device goes to the 'on' state at 0 V when using the methyl-terminated SAIM, at a high negative voltage of −18 V when using the NH_2-terminated SAIM and at a high positive voltage of +14 V when using the CF_3-terminated SAIM (see Fig. 15 *a*).

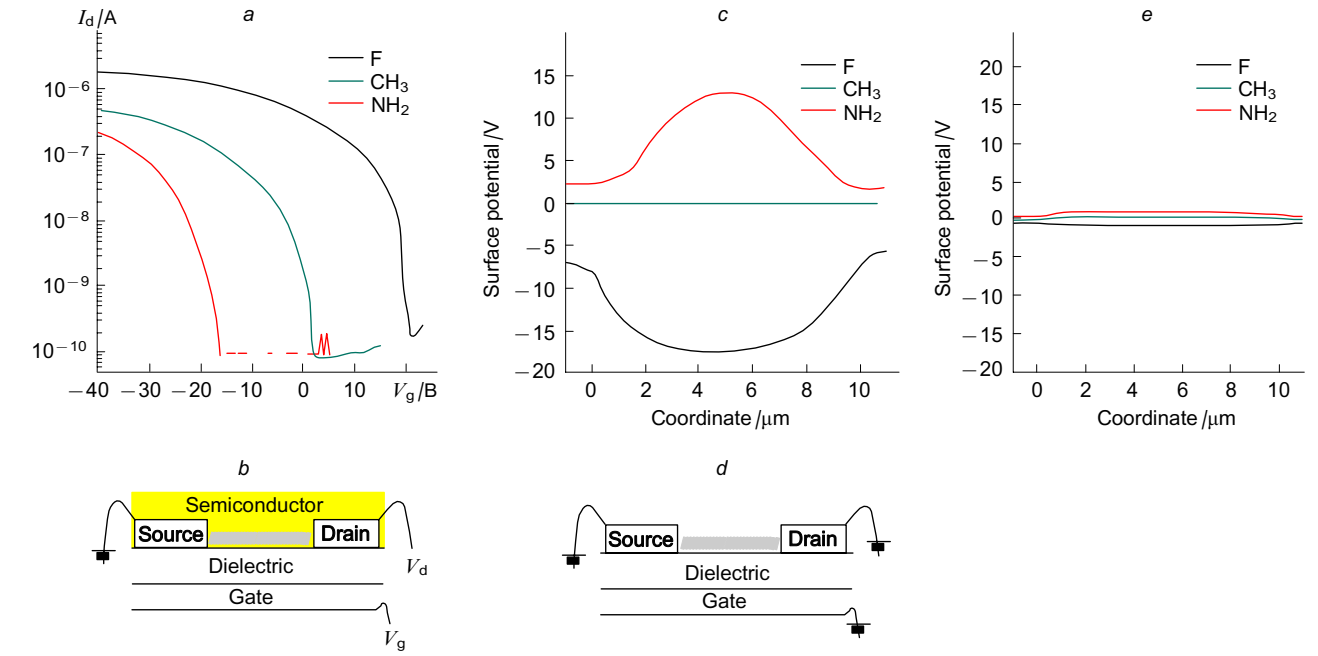


Figure 15. Dependence of electrical properties of different OFETs on the chemical structure of the SAIM.[70]
(*a*) Drain current-*vs.*-gate voltage plots (OFET layout (*b*); (*c*) surface potential distribution for OFETs with different SAIMs upon removal of semiconductor layer (OFET layout *d*); (*e*) surface potential distribution between the drain and source electrodes on dielectric surface for OFETs with different SAIMs upon removal of semiconductor layer.

To disclose the reasons for such a large shift of the threshold voltage, the following was made. The transfer characteristics of the SAIM-modified OFET were determined and then the semiconductor layer was removed from the substrate surface using a Scotch tape and the surface potential distribution in the OFET channel was studied by SKPM (see Fig. 15 *c*). It was established that the SAIM has strong effect on the potential distribution. Namely, there is zero potential in the OFET channel for the methyl-terminated SAIM, a negative potential for the CF_3-terminated SAIM and a positive potential for the NH_2-terminated SAIM. Numerical calculations showed that so high residual potentials cannot be due to the dipole moments of the SAIM molecules. A study of the substrate coated with interface layer without preliminary electrical measurements confirmed the results of numerical simulation and the potential in the channel was at most 2 V (see Fig. 15 *e*). Having analyzed the dependences of the potential in the OFET channel on time and the influence of the relative humidity of air on the time dependence of the potential, the authors[70] concluded that the shift of the threshold voltage is due to trapping of charge carriers by the interface layer in the course of measurements. The key practical result obtained was demonstration of the possibility to shift the threshold voltage using different SAIMs.

Yet another important function of the SAIM is modification of dielectric gate surface to reduce the density of charge carrier traps. This approach was successfully used in experimental studies using SAIMs of different chemical nature.[71–74] An SKPM study of charge trapping in the OFET channel by the SiO_2 dielectric and of the influence of SAIMs on the surface electronic states reported by Salmeron and co-workers[75] deserves particular attention. A quinquethiophene derivative, 4-(5-decyl-2,2′;5′,2″;5″,2‴;5‴,2⁗-quinquethiophen-5⁗-yl)butanoic acid (D5TBA), was used as the semiconductor layer. This material was chosen considering the high electrical properties characteristic of oligothiophenes and on the presence of hydrophilic carboxyl group in the parent compound, which enabled fabrication of the semiconductor monolayer by the Langmuir—Blodgett method. A bottom-gate bottom-contact OFET was studied (300-nm thick silica layer and 10 μm long and 1000 μm wide channel). After transfer of the semiconductor, the samples were kept in argon atmosphere for 24 h to remove residual water. SKPM measurements were carried out in nitrogen atmosphere at a relative humidity of less than 0.5%. To calculate the density of surface states at the dielectric/semiconductor interface, the OFET was analyzed using the parallel-plate capacitor model. The density of states was defined as

$$N = \frac{c}{hq}\left[(V_g - V_t) - V_{sf}\right] \qquad (2)$$

where c is the capacitance of the dielectric layer, h is the thickness of the dielectric layer, q is the elementary

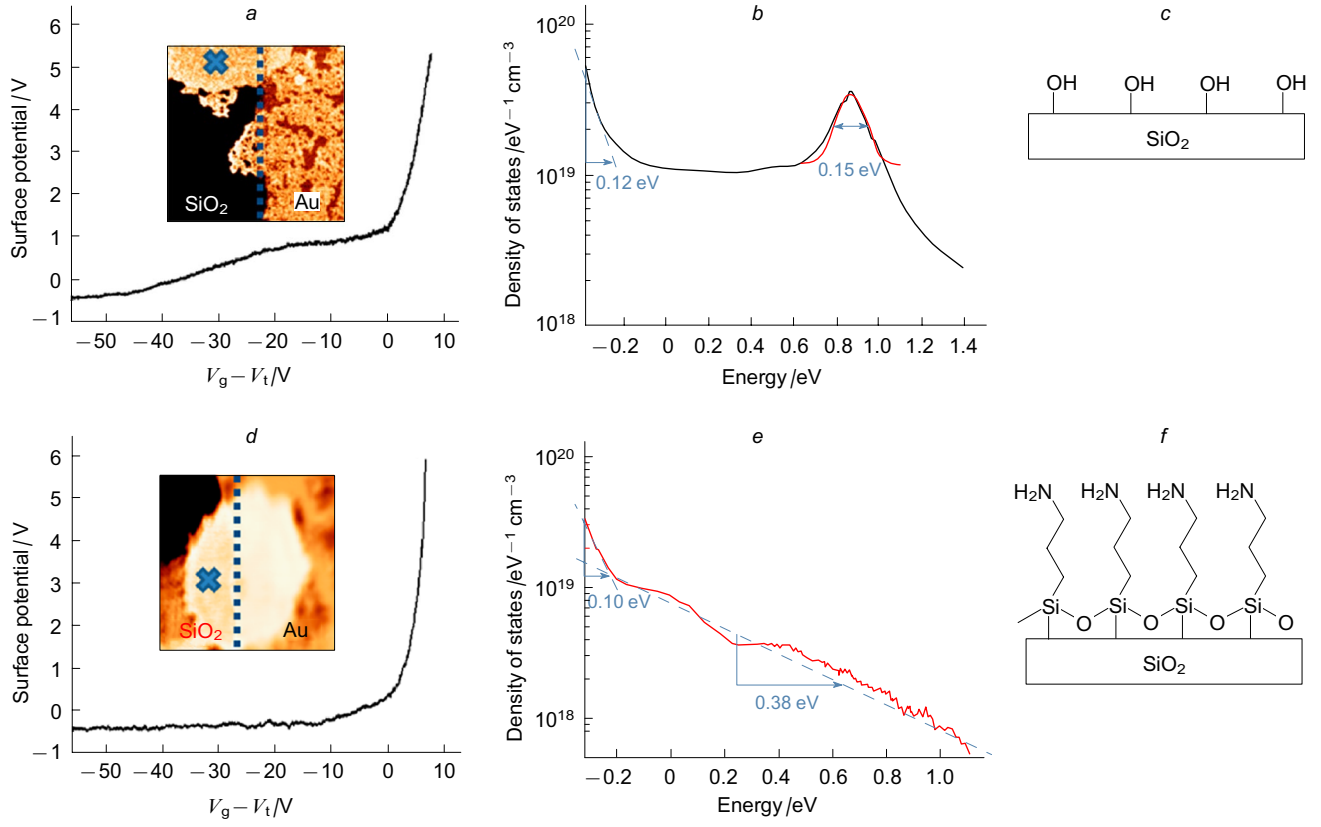


Figure 16. Plots of surface potential *vs.* gate voltage for OFETs on untreated (*a*) and on modified APTS substrate (*d*) and corresponding densities of electronic states (*b*, *e*) and chemical structures (*c*, *f*) of the substrates.[75]

charge, V_g and V_t are the gate voltage and the threshold voltage, respectively, and V_{sf} is the local surface potential. Since the energy and potential are interrelated, *viz.*, $E = qV_{sf}$, the density of states in the OFET channel is given by

$$\frac{dN}{dE} = \frac{c}{hq^2}\left[\left(\frac{dV_{sf}}{dV_g}\right)^{-1}\right] \quad (3)$$

Thus, SKPM measurements of the dependence of V_{sf} on V_g gave information on the density of states in the OFET (Fig. 16). The gate bias was set to 0 V to allow V_t for equilibration before acquiring each next spectrum. The gate voltage was varied at a rate of 10 to 20 mV s^{-1} and the probe was located 10 nm above the surface. First, the nontreated OFET was tested (see Fig. 16 *c*). The point above the semiconductor domain, at which the surface potential was measured, is shown in the inset in Fig. 16 *a*. The dependence of the surface potential on the gate voltage is essentially nonlinear (see Fig. 16 *a*). Nevertheless, there is a linear portion at $V_g - V_t > 0$, which is due to the absence of electronic conductivity in D5TBA. At -18 V $< V_g - V_t < 0$, the surface potential takes a constant value. At $V_g - V_t < -18$ V, it somewhat decreases and then again takes a constant value owing to injection of charge carriers and screening of the gate potential. The surface potential distribution for the nontreated OFET was plotted using expression (3) for the density of states. The plot in Fig. 16 *b* demonstrates the valence band (portion of the curve with a 'slope' of 0.12 eV, which agrees with published data) and a density of states peak at 0.87 eV, which was associated with the presence of hydroxyl groups on the silica surface. To prove this assumption, the substrates were modified by the APTS SAIM (see Fig. 16 *f*). The existence of the monolayer was confirmed by XPS, AFM and CA measurements. Like for the untreated substrate, the surface potential was studied as function of gate voltage. At $V_g - V_t > 0$, the plot is linear since the D5TBA film exhibits no electronic conductivity. At $V_g - V_t < 0$, the surface potential slowly decreased to a value of 0.4 V equal to the corresponding value for the untreated substrate. Calculations of the density of states spectrum (see Fig. 16 *e*) revealed no peak at 0.87 eV originating from OH groups; however, the valence band peak still remained and was associated with the highest occupied molecular orbital (HOMO) level of D5TBA. The characteristic energy of this peak was -0.10 eV, being close to the value obtained for the unmodified substrate. At the same time, the density of states spectrum of the modified substrate obeyed a monoexponential pattern with a characteristic energy of 0.38 eV, which was associated with bulk charge traps in silica. Thus, the method for measuring the local density of states in monolayer OFETs by SKPM was developed [75] and the possibility to suppress charge trapping on silica surface using SAIMs (*e.g.*, APTS) was demonstrated.

The influence of the chemical structure of SAIMs based on carboxylic acids on the electrical properties of OFETs was studied.[76] Researchers from France used pentacene as semiconductor and alumina, Al_2O_3, as dielectric (this oxide is promising for applications in flexible organic electronic devices). The interface layers were fabricated from carboxylic acids of the general formula $CH_3(CH_2)_nCOOH$ (n = 9, 14, 18). The formation of SAIMs on the alumina surface was confirmed by AFM, XRD and CA measurements. It was shown that the alkyl chains of molecules of the monolayer are slightly tilted relative to the normal to the substrate surface. The most homogeneous SAIMs were formed using long-chain alkyls (n = 18, arachidic acid). It should be noted that the electrical properties of the untreated transistor significantly deteriorated with time, whereas the SAIM-modified devices showed high reproducibility and stability of characteristics. Also, OFETs modified by SAIMs based on the acids studied demonstrated much better characteristics compared to the multilayer analogues. Summing up, it was concluded [76] that SAIMs allow one to increase the charge carrier mobility in OFETs and to improve certain electrical parameters of OFETs, *e.g.*, stability and reproducibility of characteristics.

6. Self-assembled interface monolayers as work function modifiers

Improvement of injection of charge carriers in organic and hybrid electronic devices is a topical issue.[14, 18, 77, 78] Solution to this problem implies optimization of mutual positions of the HOMO and LUMO levels of the organic semiconductor and the electrode Fermi level. The electrode work function can be modified in different manner, *e.g.*, transition metal oxide layers,[79, 80] polymeric [77, 81] and oligomeric SAIMs.[82] We will consider the last two approaches.

Alkanethiols belong to materials that are most widely used to fabricate SAIMs as work function modifiers.[23, 83 – 86] Thiols can form covalent bonds with Au atoms (gold is often used to form conductive structures in nanoelectronics); therefore, thiol groups allow alkanethiols to form dense SAIMs on Au^{III} surface. One of the first studies on the application of thiols for modification of OFET electrodes was reported by Biscarini and coworkers.[83] They used n-alkanethiols with the chain length n varying from 3 to 16 and systematically investigated the electrical properties (in particular, charge carrier mobility) of bottom-gate bottom-contact pentacene OFETs as function of n. The SAIM-modified OFETs exhibited the following features:

— odd-even effect for charge carrier mobility;†

— well-defined maximum at n = 8 for the dependence of charge carrier mobility on n;

— exponential decrease in charge carrier mobility at large n values, which indicated a paramount importance of charge carrier injection through the SAIM for the electrical properties of OFETs.

The morphology of the semiconductor layer was studied by AFM and SKPM and the results obtained were explained as follows. Nucleation and subsequent growth of pentacene film on the electrode surface differs significantly from analogous processes occurring in the OFET channel; as a consequence, a near-electrode tran-

† The odd-even effects were many times demonstrated for different SAIMs on Au^{III} surface;[87, 88] however, the direct influence of these effects on characteristics of nanoelectronic devices was for the first time reported in Ref. 83.

sient region appears. To provide efficient charge transport, the boundary of the transient region should be in immediate vicinity of electrodes, which can be provided by fabricating a SAIM. Besides, an increase in n causes the boundary of the transient region to shift towards the electrode and the barrier for charge carrier injection to increase. Taking account of these two factors, the best properties of SAIMs were obtained at $n = 8$. Observation of the odd-even effect was explained by alternating changes in the mutual orientation of the terminal C–C bond in the alkyl chain and the organic semiconductor molecules upon successive elongation of the alkyl chain.

Alkanethiols with different end groups have been intensively studied.[86,89] For instance, Biscarini and coworkers[86] proposed a series of SAIMs based on hydroxyl-terminated n-alkanethiols ($n = 3$, 4, 6, 8, 9 and 11) for modification of OFET electrodes. Like in the previous study,[83] the existence of optimum, from the standpoint of electrical properties of the OFET, length of the alkyl spacer ($n = 4$, 6) was established. Improvement of electrical properties was associated with SAIM-facilitated minimization of the contact resistance at the semiconductor/electrode interface and with the formation of the most homogeneous morphology of the semiconductor layer that was fabricated at the SAIM–modified electrode boundary by thermal evaporation.

In addition to thiols, SAIMs based on phosphonic acid derivatives have also found application in nanoelectronics.[16,90–92] For instance, a series of TAA-based compounds capable of forming SAIMs on ITO surface through chemisorption were proposed.[16] TAA was chosen since it can form semiconductor films with hole conductivity. TAA-Modified electrodes were used in polymeric OLEDs. The SAIMs were studied by AFM, CV, CA measurements, and their efficiency in OLED application was also studied. The TAA-SAIM-modified electrodes demonstrated much higher injection of main charge carriers (holes) than oxygen plasma treated electrodes. Such a modification decreased the OLED on-voltage by 3 V compared to the unmodified ITO. It was found that the chemical structure of the starting TAA derivative used as SAIM precursor has strong effect on such properties of the monolayer as hole conductivity, electron(hole)-blocking properties and the dipole moment. It was concluded that all these properties should be taken into account in the design of electronic devices.

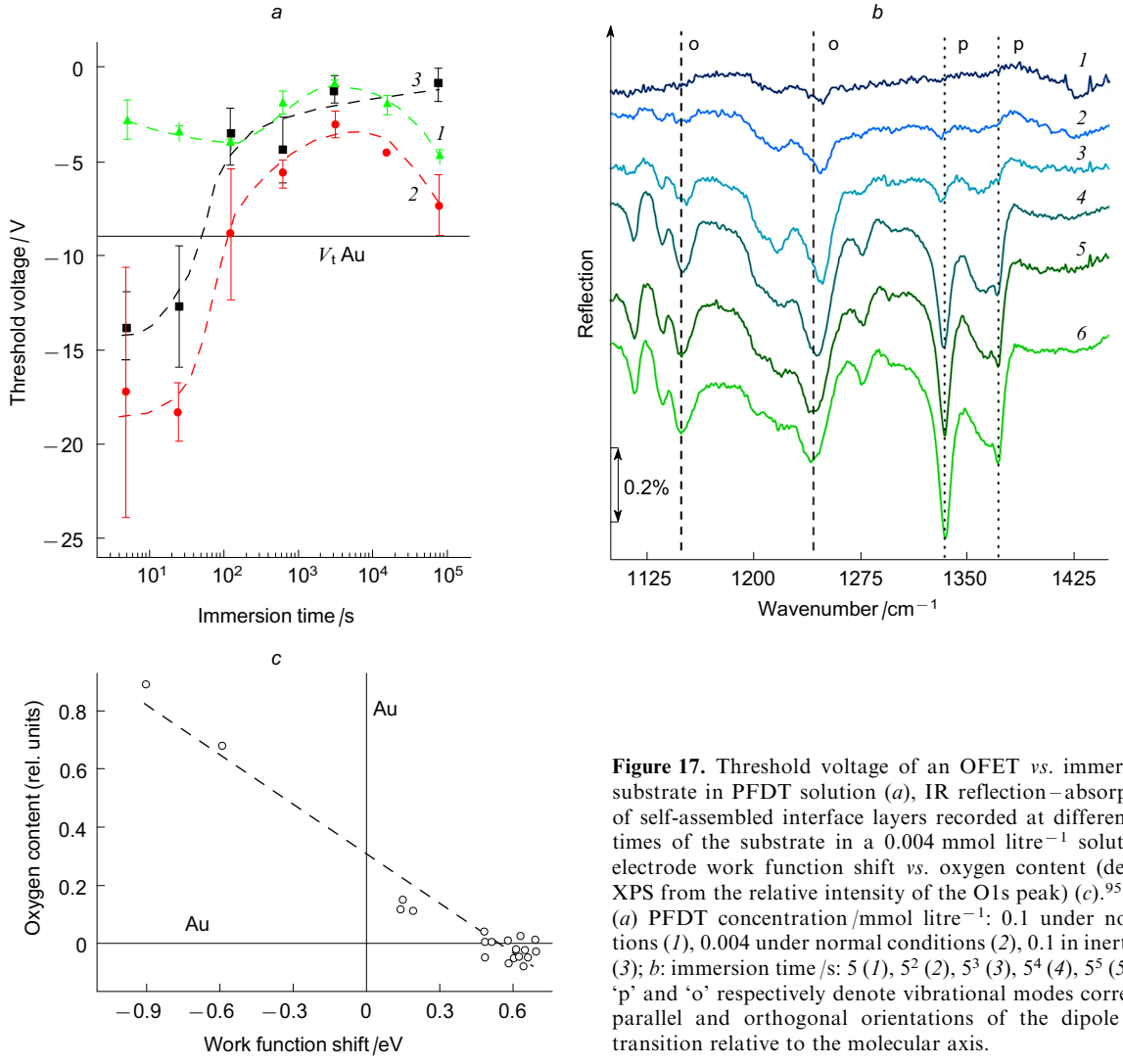


Figure 17. Threshold voltage of an OFET *vs.* immersion time of substrate in PFDT solution (*a*), IR reflection–absorption spectra of self-assembled interface layers recorded at different immersion times of the substrate in a 0.004 mmol litre^{-1} solution (*b*), and electrode work function shift *vs.* oxygen content (determined by XPS from the relative intensity of the O1s peak) (*c*).[95]
(*a*) PFDT concentration /mmol litre^{-1}: 0.1 under normal conditions (*1*), 0.004 under normal conditions (*2*), 0.1 in inert atmosphere (*3*); *b*: immersion time /s: 5 (*1*), 5^2 (*2*), 5^3 (*3*), 5^4 (*4*), 5^5 (*5*), and 5^6 (*6*); 'p' and 'o' respectively denote vibrational modes corresponding to parallel and orthogonal orientations of the dipole moment of transition relative to the molecular axis.

Fluorinated alkanethiols as SAIM precursors were studied.[23,93–96] In most cases, SAIMs prepared by long-term solution deposition (> 10 h) were described; the starting compounds were stored and processed in controlled atmosphere. A study[95] of 1*H*,1*H*,2*H*,2*H*-perfluorododecanethiol (PFDT) as SAIM precursor involved experiments on SAIM formation on the surface of Au electrodes upon rapid (from a few seconds) immersion in a PFDT solution in the presence of trace amounts of oxygen. It was shown that the choice of conditions for fabrication of SAIMs with necessary functionality remains topical. The SAIMs prepared were studied by XPS, IR spectroscopy, ultraviolet photoemission spectroscopy (UPS) and by measuring the electrical properties of the SAIM-modified OFETs. In Fig. 17 *a* the threshold voltage of the OFET with SAIM-modified electrodes is plotted *vs.* immersion time of substrate in PFDT solution under different conditions. The threshold voltage decreased and the charge carrier injection into the semiconductor layer improved with increasing immersion time. In addition, the dependence of V_t on immersion time for the SAIM fabricated under normal conditions demonstrated saturation that was explained by gradual degradation of the SAIM owing to partial oxidation of the SAIM molecules at long immersion times. Mention was made that a similar effect was well studied in a publication devoted to environmental hazards of hydrofluorocarbons.[97] Interestingly, experiments with sufficiently high initial concentration of the solutions under normal conditions led to rather large shifts of the threshold voltage even at very short immersion times (5 s), whereas the closest-to-zero V_t values were observed at immersion times in the range of $10^3 - 10^4$ s.

Infrared reflection–absorption spectra of a PFDT solution deposited SAIM on Au surface (initial solution concentration was 0.004 mmol litre^{-1}) are shown in Fig. 17 *b*. It was found that at short immersion times the spectral pattern does not correspond to the presence of a dense SAIM on the Au surface; this was additionally confirmed by the results of measurements of the properties of a top-gate bottom-contact OFET. Only at immersion times $> 5^3$ s the spectral pattern corresponded to a dense SAIM with alkyl chains slightly tilted from the normal to the substrate surface. The tilt angle of fluorinated alkyl chains in dense SAIM determined by comparing the IR spectroscopy and XPS data was $10 \pm 3°$. It was reported that trace amounts of oxygen have strong effect on the properties of the SAIMs stored under normal conditions upon modification. The UPS data (see Fig. 17 *c*) show that the work function shift depends on the content of oxygen. Noteworthy, at rather high oxygen content the work function can be shifted towards higher values. This not only levels the effect of electrode modification by the SAIM, but can also deteriorate the

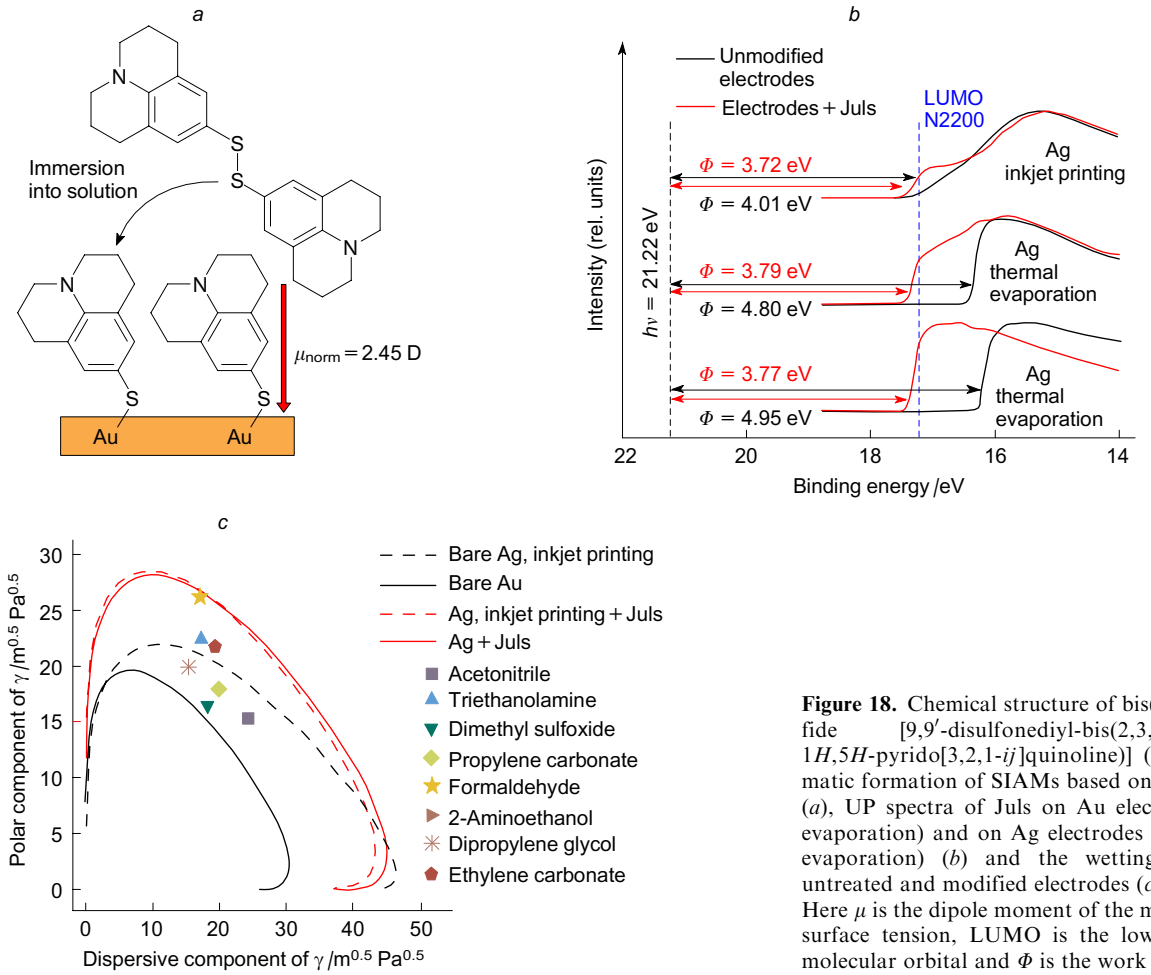


Figure 18. Chemical structure of bis(julolidyl) disulfide [9,9′-disulfonediyl-bis(2,3,6,7-tetrahydro-1*H*,5*H*-pyrido[3,2,1-*ij*]quinoline)] (Juls) and schematic formation of SIAMs based on this compound (*a*), UP spectra of Juls on Au electrodes (thermal evaporation) and on Ag electrodes (inkjet, thermal evaporation) (*b*) and the wetting envelopes of untreated and modified electrodes (*c*).[104]
Here μ is the dipole moment of the molecule, γ is the surface tension, LUMO is the lowest unoccupied molecular orbital and Φ is the work function.

injection behaviour compared to the bare electrodes. In spite of this, practical applicability of the OFET electrode modification by PFDT-based SAIMs was pointed out. Indeed, the OFET demonstrated high operating characteristics for long time owing to encapsulation of the SAIM fabricated by successive formation of the semiconductor and dielectric layers and the gate electrode.

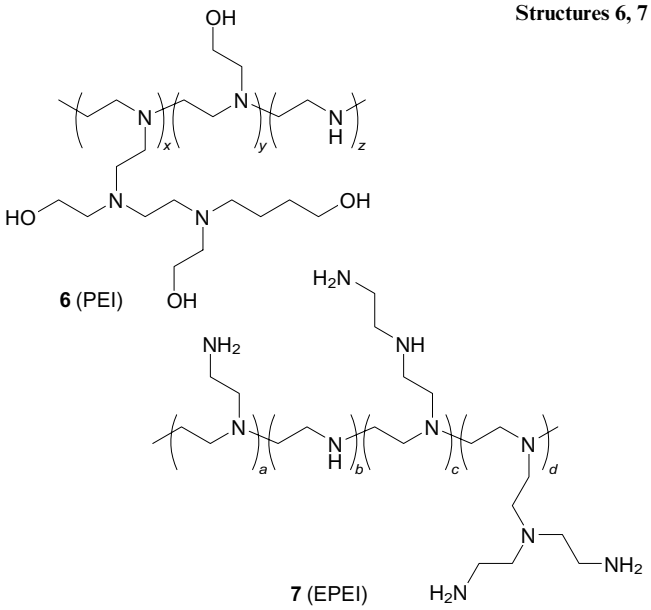
Practically valuable features of SAIM molecules include the dipole moment suitable for changing the electrode work function and the surface properties, in particular, the surface wettability. The requirements imposed on wettability are due to the need for formation of subsequent layers on the SAIMs using fast solution techniques, *e.g.*, inkjet printing. Recently, SAIMs based on aromatic and π-conjugated compounds have been intensively studied to improve wettability.[92, 98 – 105] Aromatic fragments in the SAIM structure provide more efficient charge transport across the interface layer and charge injection.[106]

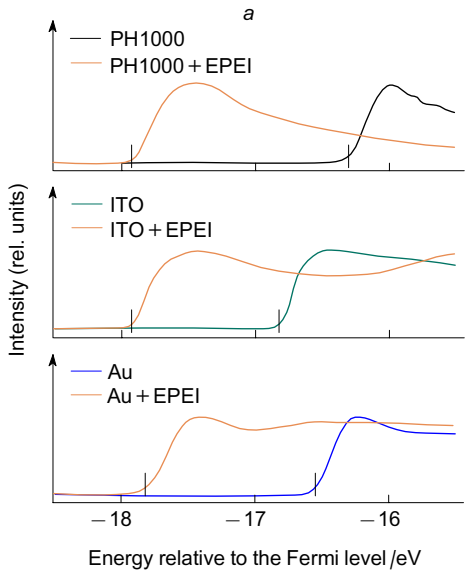
A thiolate, namely, bis(julolidyl)disulfide [9,9′-disulfanediylbis-(2,3,6,7-tetrahydro-1*H*,5*H*-pyrido[3,2,1-*ij*]quinoline)] (Fig. 18 *a*) was proposed[104] as precursor for work function modifier SAIM to modify Au electrodes fabricated by thermal evaporation and silver electrodes fabricated by thermal evaporation and inkjet printing. Self-assembled interface layers based on this compound were prepared by solution deposition at different immersion times (from 1 to 120 min). The SAIMs were studied by XPS, IR spectroscopy, UPS, CA measurements and by measuring the electrical properties of the SAIM-modified OFETs. It was shown that immersion for 1 min is sufficient to achieve highly efficient operation of the SAIM-modified OFET. UPS experiments revealed that the SAIMs thus prepared provide a decrease in the electrode work function of up to 1.2 eV (see Fig. 18 *b*). This allows one to use these electrodes in n-type transistors (in particular, the N2200 organic semiconductor was used). The wettability of the electrodes was assessed using the so-called wetting envelopes (see Fig. 18 *c*).[107] Based on their analysis, it was concluded that SAIMs provide better wettability compared to the bare electrodes. Taking account of high modification rate the approach proposed seems promising for fabrication of flexible electronic devices using printed techniques.

In addition to low-molecular-mass functional compounds, polymers are also used as SAIM precursors.[4, 77] Researchers from the group headed by Prof Kippelen proposed[81] a universal method for fabricating low work function electrodes for organic electronics, which is based on physical adsorption of a thin layer (1 – 10 nm thick) of a polymer containing amino groups onto the surface of an electrode. Such a polymer exhibits the properties of a dielectric, thus being an electrode surface modifier rather than injection layer. As the electrode surface is coated with a thin polymer layer, self-assembled molecular dipoles contribute to the total dipole moment of the interface layer and thus change the work function of the electrode.

The SAIM precursors, branched polyethyleneimine (**6**) and ethoxylated polyethyleneimine (EPEI, **7**), were chosen owing to high content of amino groups, which allowed one to expect large dipole moments of corresponding layers. UPS measurements of the work function

Structures 6, 7





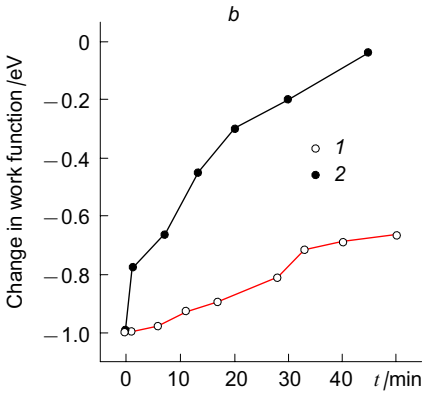


Figure 19. UPS spectra of conductive electrodes made of different materials before and after modification by EPEI (*a*) and changes in the work function of ITO electrodes upon immersion in water (*1*) and under sonication (*2*) (*b*).[81]

of conductive electrodes made of different materials were carried out before and after modification by EPEI. The results obtained are presented in Fig. 19 *a*. The UPS spectra exhibit a decrease in the work function from 4.95 to 3.32 eV for the electrode based on a mixture of poly(3,4-ethylenedioxythiophene) and poly(styrene sulfonate) (PEDOT:PSS, PH1000 grade), from 4.4 to 3.3 eV for ITO and from 4.7 to 3.4 eV for Au. These results were confirmed by SKPM. The results of the SAIM stability studies involving immersion in water and sonication are shown in Fig. 19 *b*). The longer the immersion time of the modified ITO-electrodes in water the higher the electrode work function. Nevertheless, the resilience of the SAIM on the surface even at long immersion times (50 min) was indicative of rather strong interaction between the polymer film and the electrode. Contrary to this, sonication led to complete removal of fhe EPEI layer; therefore, the interaction between the SAIM and the electrode was weak. The authors [81] believed that such a weak interaction allows one to consider this modification method as universal and applicable to all electrode materials. This was demonstrated taking tailored organic electronic devices (inverted solar cells and OFET with n-type semiconductor) as examples. Both devices were characterized by good electrical properties due to electrode modification by the SAIMs proposed; this pointed to practical value of the approach in hand.

Concluding this Section, mention may be made that modification of electrode work function is one of the best studied aspects of the application of SAIMs in electronics. To date, a huge number of compounds have been tested as SAIM precursors. There is increasing number of studies devoted to not only a decrease in the work function, but also improved processability of methods for fabrication of SAIMs and optimization of their surface properties for more efficient formation of subsequent layers using solution methods including inkjet printing. It is expected that in the nearest future SAIMs as work function modifiers will be widely used in organic electronic manufacturing technologies.

7. Self-assembled interface monolayers for surface modification of organic semiconductors

Surface modification of organic semiconductors is an interesting application of SAIMs.[96,108–113] The possibility to grow SAIMs on the surface of organic single crystals was for the first time demonstrated by Podzorov and co-workers,[96] who studied three organosilicon compounds, namely, (tridecafluoro-1,1,2,2-tetrahydrooctyl)-trichlorosilane (FTS), n-octyltrichlorosilane (OTS) and (tridecafluoro-1,1,2,2-tetrahydrooctyl)triethoxysilane (FTES) as the SAIM precursors. The model semiconductors were single-crystalline rubrene and tetracene having p-type conductivity.[114] In the experiments a chamber containing an organic semiconductor (SC) crystal with thermally evaporated Ag electrodes (see inset in Fig. 20 *a*) was filled with a solution of SAIM precursor and the time dependence of the current flowing through the sample at constant voltage was measured. The formation of the SAIM on the surface of organic SC was followed by the appearance of a region with high hole density and the current increased with time. The current-*vs*.-time plot had the shape of a saturation curve while

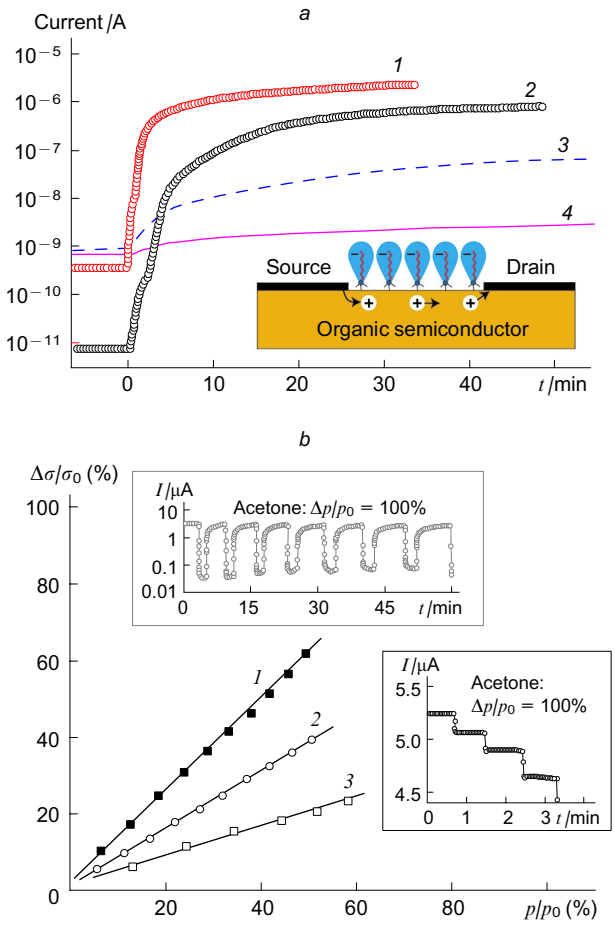


Figure 20. Electric current in rubrene and tetracene single crystals *vs*. time at a d.c. voltage (*a*) and changes in relative conductivity of rubrene single crystals with different interface layers (FTS and OTS) *vs*. relative vapour pressure of acetone and isopropyl alcohol (p_0 is saturated vapour pressure) (*b*).[96]
(*a*) FTS, rubrene (*1*); FTS, tetracene (*2*); ethoxysilane, rubrene (*3*); OTS, rubrene (*4*);
(*b*) FTS, rubrene: acetone (*1*); OTS, rubrene: acetone (*2*); FTS, rubrene: propanol (*3*).

the maximum surface conductivity (σ) was dependent on the type of the SAIM precursor. The maximum surface conductivity was 10^{-5} S per square, which is comparable with the record high conductivity values for OFETs.[115] It was established that the higher the fluorine content in the SAIM molecule the more pronounced the semiconductor doping effect. In addition, the presence of a reactive group [$SiCl_3$, $Si(OEt)_3$ or COOH] in the precursor molecule is crucially important for the onset of the doping effect.

SAIM-Modified OFETs can be used as selective gas sensors. A study [109] of the interaction of doped organic single crystals with acetone, propanol, ethanol, xylene, chlorobenzene and water vapours showed that the response to these gases consists in the change in the relative conductivity ($\Delta\sigma/\sigma$) and is fast (fractions of a second) and reversible. Changes in the relative conductivity of rubrene single crystals with two different interface layers (FTS and OTS) are plotted *vs*. relative vapour

pressure of acetone and isopropyl alcohol in Fig. 20 *b*. The dependence of $\Delta\sigma/\sigma$ on the analyte pressure is linear, the slope being determined by the nature of the gas and the SAIM precursor. Interestingly, polar gases caused the SC conductivity to change over a wide range, whereas nonpolar ones (xylene, hexane and pentane) had no effect on conductivity. This effect was explained by the specific mechanism of the interaction between the gas and the SAIM. The model proposed assumes that gas molecules penetrate into the SAIM, violate the ordered structure and thus reduce the doping effect, which in turn leads to a decrease in conductivity. Nonpolar gases penetrate into SAIMs to a lesser extent than polar ones, which provides an explanation for the differences in the sensor response. It was concluded that the approach proposed is versatile and promising for the design of gas sensors based on SAIM-modified organic semiconductors.

Shin *et al.*[109] studied the possibility to optimize parameters of n-type OFETs using SAIMs. The authors of most studies on chemical modification of organic SC used SAIMs containing fluorinated fragments since such SAIMs exhibit electron-withdrawing properties. In contrast to this, Shin *et al.*[109] proposed to use two organosilicon compounds, APTS and *N*-[3-(triethoxysilyl)propyl]ethane-1,2-diamine (TEDA) containing electron-donating amino groups.[109] They assumed that SAIMs based on APTS and TEDA will improve the properties of OFETs based on n-type semiconductors, *N*,*N*′-dioctylperylene-3,4,9,10-dicarboximide (PTCDI-C8) and poly{[*N*,*N*′-bis(2-octyldodecyl)naphthalene-1,4,5,8-bis(dicarboximide)-2,6-diyl]-*alt*-5,5′-(2,2′-bithiophene)} (PNDI2OD-2T, ActivInk N2200). Bottom-gate top-contact OFETs (Fig. 21 *a*) were fabricated. Prior to depositing the SC the Si substrate with thermally evaporated SiO_2 layer (300 nm) was coated with a thin film of octadecyltrimethoxysilane (ODMS). The semiconductor was deposited by thermal evaporation (PTCDI-C8) or SCT (PNDI2OD-2T).

Experimental data demonstrating a correlation between the charge carrier mobility and the FET threshold voltages for PTCDI-C8 films of different thickness before and after modification by SAIM are presented in Fig. 21 *b*. SAIMs significantly improve the operating characteristics of all OFETs studied. For instance, treatment of the transistor in APTS vapours allows the electron mobility to increase tenfold (from 0.02 to 0.2 $cm^2\ V^{-1}\ s^{-1}$) and the threshold voltage to decrease from 20 to 6 V. It was pointed out that the dependences of the key parameters of the devices on the exposure time to fumes have the shape of saturation curves and that the currents flowing through the devices reach their maximum values after 60 min deposition in APTS and after 30 min deposition in TEDA. It was concluded that the efficiency of doping depends on the number of amino groups and therefore the effect of the TEDA-based SAIM manifests itself faster. At the same time, the shift of the OFET threshold voltage in the case of TEDA occurs slower than in the case of APTS. To explain this fact, diffusion of aminosilanes across the organic SC layer towards the bottom SC/dielectric interface was assumed. In the case of APTS, diffusion should occur faster owing to smaller size of the precursor molecules. Thus, the APTS molecules will arrive at the SC/dielectric interface after a shorter time and thus shift the threshold voltage of the transistor. Nevertheless, no solid arguments in favour of this mechanism were presented, whereas other possible explanations for the observed trends include doping of the organic SC or improvement of charge injection from electrodes into the SC. Despite this fact, high efficiency of doping the n-type OFET with amine-terminated organosilicon compounds is an important practically valuable result. In a more recent study[116] the possibility of modifying the properties of OFETs using SAIMs was also demonstrated for p-type transistors.

Concluding this Section, it should be noted that pioneering studies on the application of SAIMs for modification of organic SC have been reported only recently (in the last decade) and this investigation line seems to be promising for progress in organic and hybrid electronics. Design of the precursor molecules allows one to vary both the electrical characteristics of devices and their properties in different atmospheres. One can expect an increase in the number of publications on this topic.

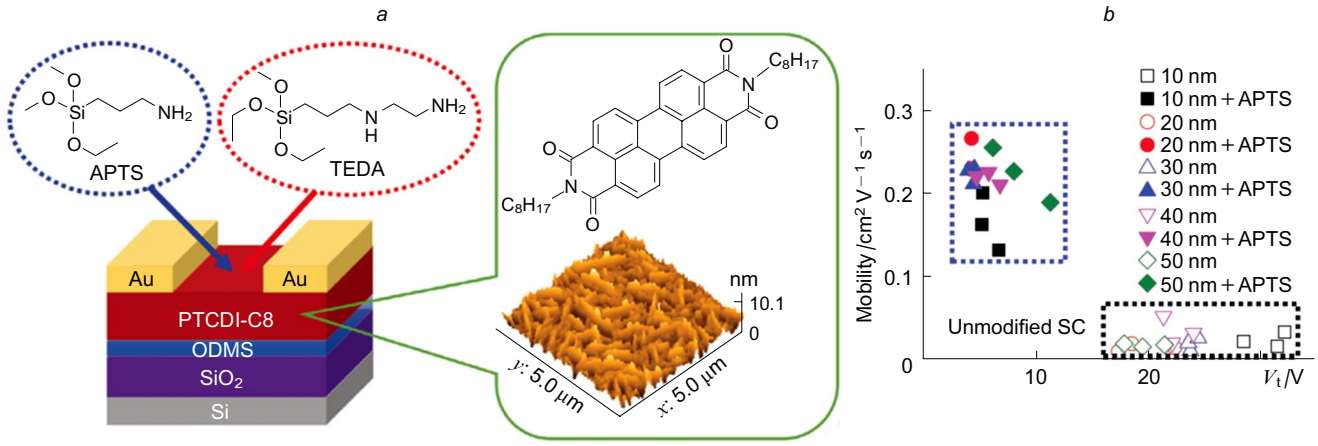


Figure 21. The n-type OFET architecture, the chemical structure of the SAIM and the SC layer (*a*) and experimental data demonstrating a correlation between the charge carrier mobility and the FET threshold voltages for untreated and SAIM-modified PTCDI-C8 films (*b*).[109]

8. Self-assembled interface monolayers for applications in biosensors

Self-assembled monolayers with end groups of different functionality are widely used in molecular biology studies and in biosensor prototypes.[117, 118] Biosensors are microelectronic devices engineered to convert biochemical interactions occurring at the sensor/liquid interface into measurable signals. Biosensor engineering is a topical avenue of modern scientific and applied research while potential application fields of biosensors include environmental monitoring, food quality control, analysis of the effect of drugs, *etc*. Interest of researchers in biosensors is due to great potential of label-free detection of biomolecules.[119] Besides, an undoubtful advantage of label-free sensors is that they can be based on a wide variety of physical methods for the detection of transducer's response (CV, quartz microbalance, electrochemical impedancemetry, *etc*.). Practical implementation of an efficient biosensing platform requires a high-accuracy control of the interface between (bio)recognition element and transducer. To this end, modern biosensors utilize organic interface layers that provide biofunctioning of substrates or conductive structures as components of transducers (see Fig. 1*f*). Efficient immobilization of (bio)sensing receptors on transducer surface and reduction of the probability of nonspecific sorption can be achieved using SAIMs. Below we will consider the most remarkable studies devoted to this area of research.

Organosilicon compounds are widely used in biosensor applications.[120 – 125] For instance, a biosensor prototype for real-time label-free detection of the interaction between biotin acting as a recognition element and avidin in buffer solution was described.[118, 122] Sensing relies on the ultrahigh frequency electromagnetic piezoelectric acoustic wave technology. The prototype [122] is a practical implementation of the previously described SAIMs based on cross-linked functional derivatives of trichlorosilanes.[126] The biosensing platform included an electrodeless piezoelectric quartz resonator disc coated with the SAIM representing a co-deposited mixture of specially synthesized pentafluorophenyl ester attached to a trichlorosilane fragment *via* a dodecyl spacer [120] and a shorter-chain monofunctional OTS molecule (Fig. 22). Then, thiolated or aminated biotin probes were grafted onto the SAIM in one step without pre-activation through specific binding to the pentafluorophenyl ester moiety. The extent of surface modification was determined from angle-resolved XPS data. The biosensing properties were evaluated using a highly sensitive electromagnetic piezoelectric acoustic sensor using micromolar buffer solutions of avidin. Non-specific adsorption was blocked by injecting bovine serum albumin.[127] The biosensor prototype demonstrated good reproducibility, which is an important step towards development of real biosensors capable of operating with more complex biological objects.

Uragami and co-workers [121] also demonstrated the possibility to use SAIMs based on organosilicon com-

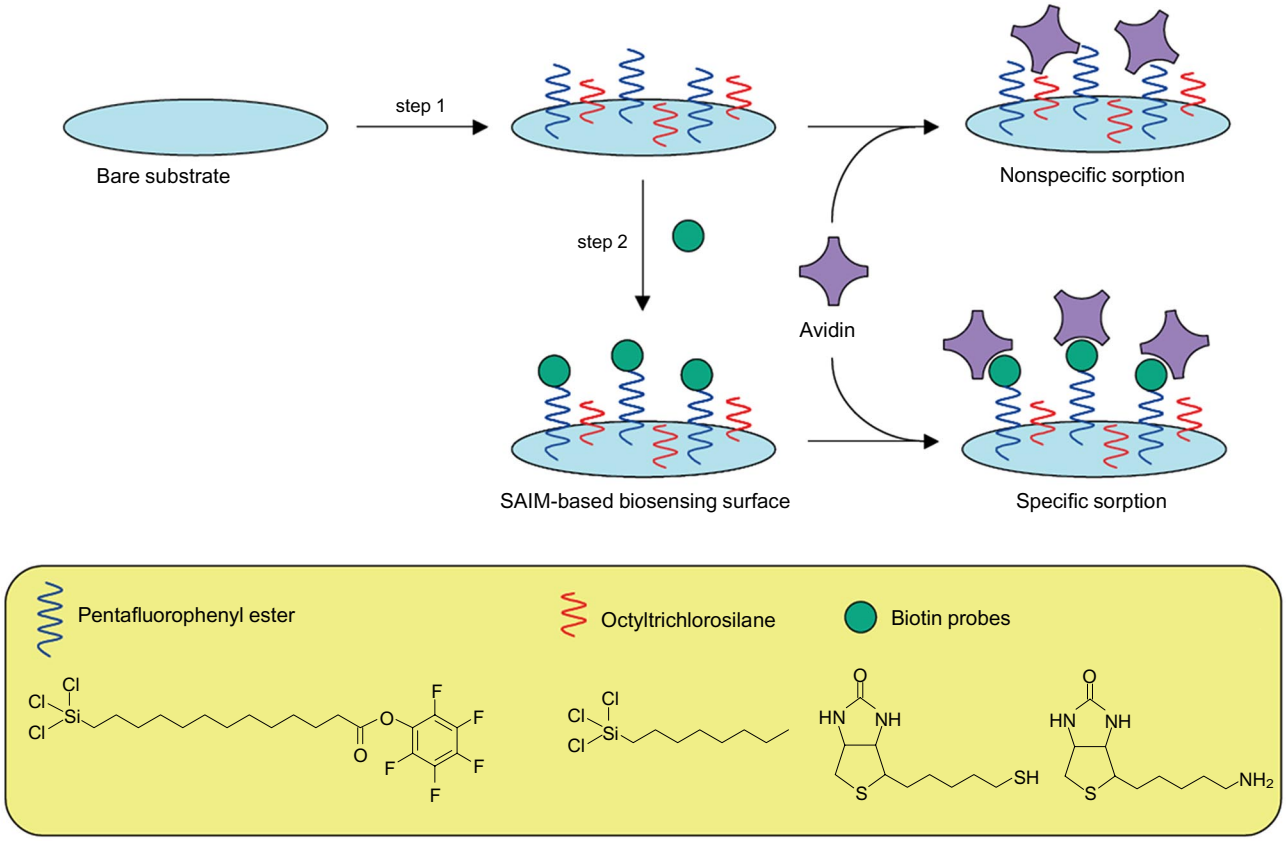


Figure 22. Scheme illustrating the preparation and operating principle of a biosensor prototype based on mixed OTS monolayer and a trichlorosilane derivative of pentafluorophenyl ester for the detection of biotin – avidin interactions.[122]

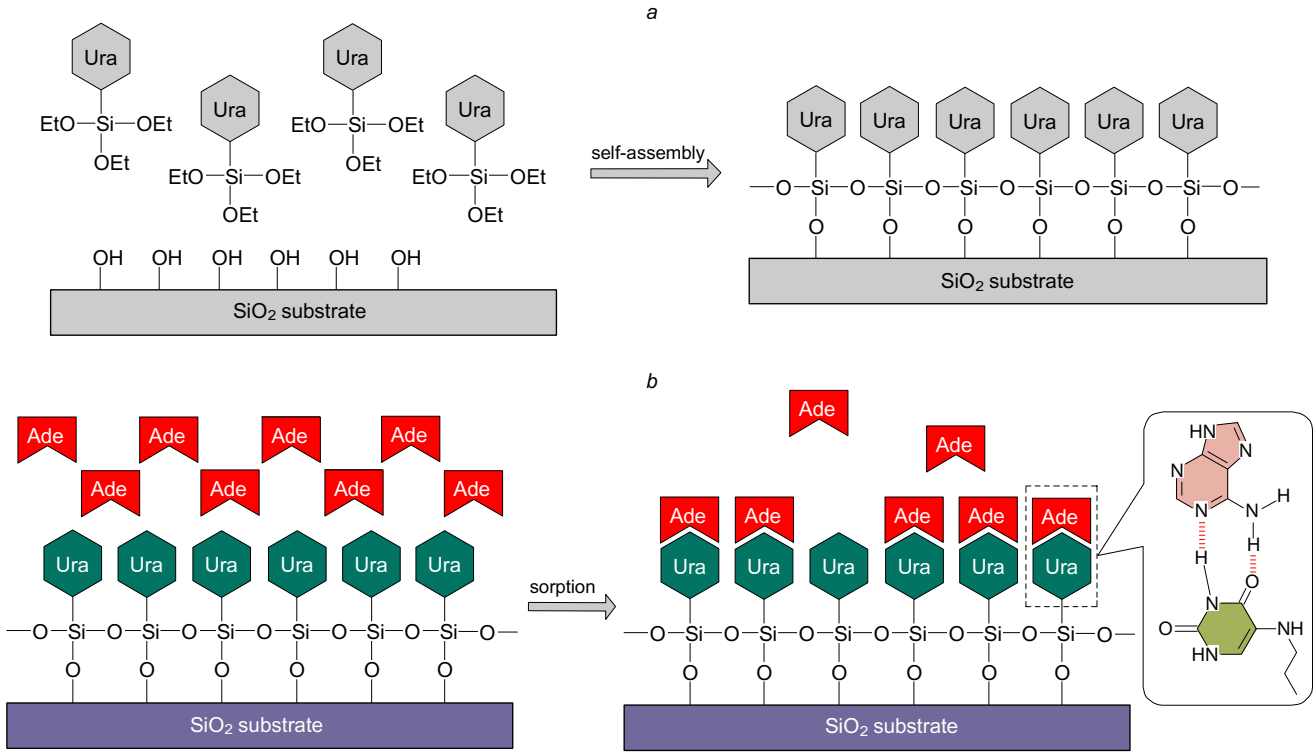


Figure 23. Schematic formation of SAIMs based on uracil-modified triethoxysilane on hydrophilized silica (*a*) and adenine sorption on the surface of uracil-modified SAIMs (*b*).[121] Ade is adenine and Ura is uracil.

pounds. A triethoxysilane derivative chosen as modifier was more stable than trichlorosilane derivatives under standard atmospheric conditions. The new nucleotide-terminated triethoxysilane was synthesized by the solvent-free reaction of 5-bromouracil with 3-(aminopropyl)triethoxysilane. The uracil-containing triethoxysilane was used as a precursor for the SAIM fabricated on hydrophilized silicon from 2 μmol litre^{-1} solution in anhydrous cyclohexanone (Fig. 23 *a*) in the presence of trace amounts of water. The SAIM was adsorbed on SiO_2 surface following a published procedure.[128] The resulting uracil-containing SAIMs were characterized by XPS and ellipsometry. The SAIM was 9 nm thick and complete surface coverage by the SAIM could be achieved within 10 h. It was shown that adenine complementary to uracil can be effectively adsorbed onto the uracil-containing surface due to the complementary hydrogen bonding (see Fig. 23 *b*) and interacts with up to 70% of the uracil fragments immobilized on the monolayer surface. As a result, it was concluded that the method based on self-assembly of nucleotide-containing carbosilanes is promising for the development of bioconjugated devices for the detection and separation of nucleotide bases and nucleic acids.

Recently, sulfur compounds have been widely used in addition to organosilicon compounds to prepare SAIMs for biosensors.[123, 129 – 136] Since thiols can form covalent bonds with Au surfaces, SAIMs based on them are utilized to modify conductive Au structures in biosensors. A strategy[132] for functionalization of Au surfaces enables covalent binding of antibodies to the transducer with high reproducibility (Fig. 24). In the first step a primary SAIM based on a mixture of 3-mercaptopropionic acid (3-MPA) and 11-mercaptoundecanoic acid (11-MUA) acid in a 10 : 1 ratio was grafted onto Au surface. The molecules with different alkyl chain lengths were chosen from the standpoint of effective immobilization of biomolecules on such SAIMs, *viz.*, the resulting SAIM structure favours sorption of biological compounds with undistorted conformations and provides a higher sorption density.[137] Next, the surface of the primary SAIM was treated with *N*-ethyl-*N*′-(3-diethylaminopropyl)carbodiimide (EDC) and sulfo-(*N*-hydroxysulfosuccinimide) sodium salt (sulfo-NHS) containing carboxyl groups. This led to formation of a hybrid SAIM on the Au surface. In the third step the antibodies chosen (anti-lgG and anti-lgM) were covalently bound to the SAIM carboxyl groups through the amino groups. In the final step the unreacted reactive groups were blocked using ethanolamine. The biosensing surfaces thus fabricated were studied by XPS, AFM, CV and electrochemical surface plasmon resonance. Based on the results obtained, it was concluded that the structure of the organic layer formed on the Au surface corresponded to the expected one. OFETs are also described in which the gate electrode was modified in accordance with the proposed approach. The OFETs thus fabricated operated in a liquid medium, while the SAIM with antibodies influenced the OFET threshold voltage. This biosensing platform is promising for the development of biosensor prototypes.

A serious limitation for practical use of SAIMs based on sulfur compounds in biosensor applications is their relatively low stability even under normal conditions.[138, 139] Therefore, the search for a promising alternative to thiols is highly relevant. A comparative study of

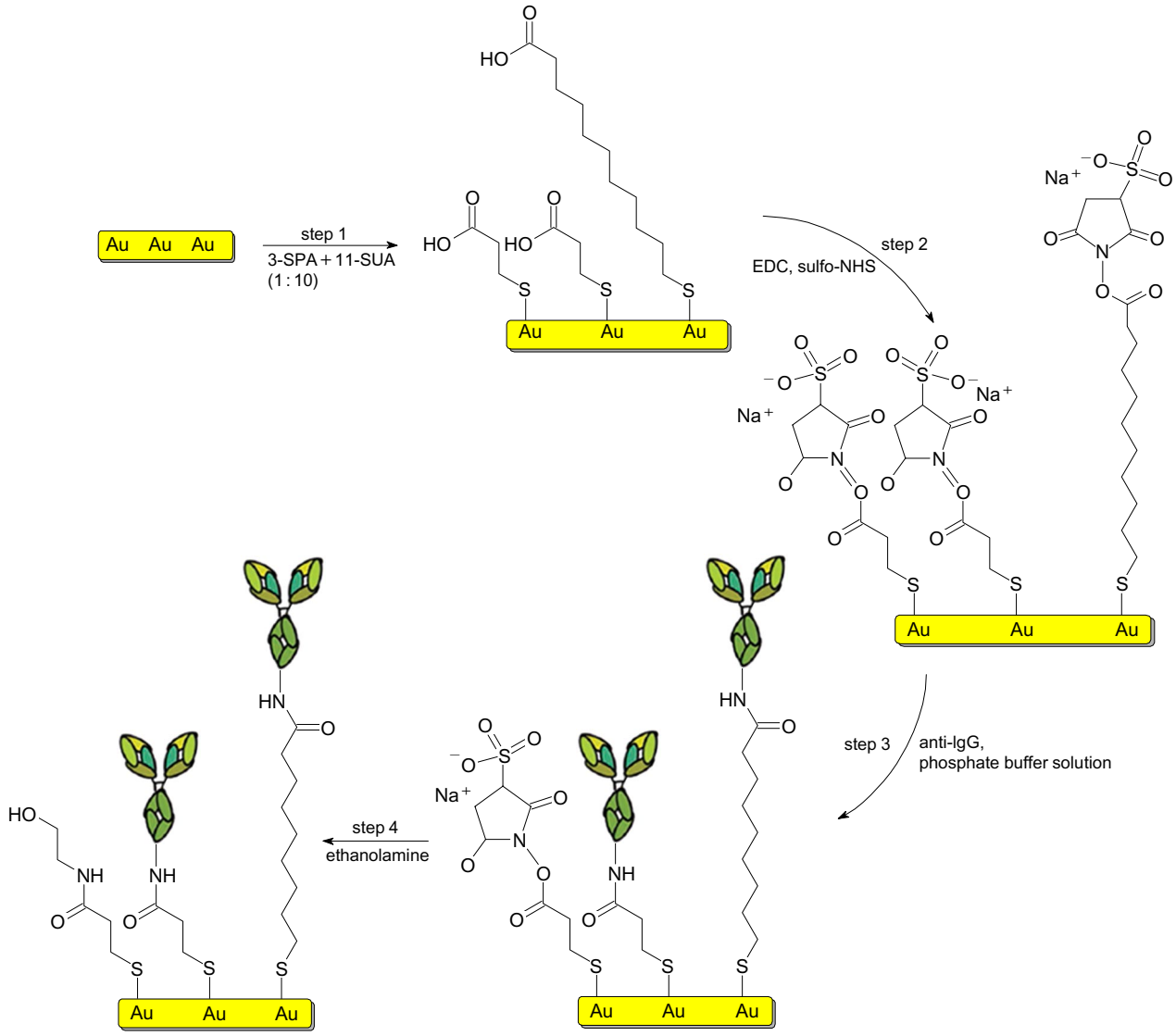


Figure 24. Stepwise formation of biosensing surface containing SAIMs on gold electrode.[132] The antibodies, anti-IgG and anti-IgM, are shown in green.

the SAIMs based on carboxymethylated dextran with two different anchor groups, namely, commercially available thiols and *N*-heterocyclic carbenes was reported.[133] The SAIMs fabricated were studied by XPS, AFM and CA measurements. The biosensor based on N-heterocyclic carbenes demonstrated higher thermal stability than that based on thiols. At the same time, the sensing properties assessed using surface plasmon resonance were independent of the type of the anchor group. It was concluded that the SAIMs prepared can be used for effective immobilization of various ligands and that the biosensing platform developed is promising for practical application.

Concluding this section, it should be noted that SAIMs play a key role in modern biosensors since they provide more effective immobilization of the (bio)recognition element on the transducer surface and make non-specific sorption on the surface of SAIM less probable. One can expect high research activity in this field in the nearest future.

9. Conclusion

At present, SAIMs and self-assembled interface ultrathin layers a few monomolecular layers thick are widely used in organic and hybrid electronics. Although they belong to auxiliary elements in corresponding systems, such layers favour efficient operation of the main functional layers. Note that most modern organic and hybrid electronic devices include one or more SAIMs, which confirms the high relevance of research on the title topic.

One of the best studied applications of SAIMs in electronic devices is associated with changes in the work function of conductors. To date, a huge number of compounds have been studied as SAIM precursors. More and more attention is being paid not only to quantitative aspects of changes in the work function, but also to improvement of methods for preparation of SAIM modifiers and optimization of their surface properties in order to create prerequisites for more efficient formation of subsequent layers on the SAIMs using

solution methods including inkjet printing. The focus of studies on self-assembled interface layers for monolayer and hybrid dielectrics shifted to SAIM-modified multilayer hybrid dielectrics, which enables precise control of the surface and dielectric properties of the films and leads to significant improvement of the characteristics of FETs that serve as the basis for microelectronic devices. The interface layers often allow one to significantly increase the charge carrier mobility and to improve the stability of FETs and reproducibility of results obtained. Recently, studies on SAIMs as surface modifiers of organic semiconductors have appeared. Targeted design of precursor molecules allows one to vary the electrical characteristics of devices in atmospheres of different composition over a wide range.

Self-assembled interface layers are also widely used to change the surface properties of polymeric substrates and to improve adhesion of conductive structures. Indeed, SAIMs allow one to combine a nearly 100% adhesion of conductive structures to chemically inert polymeric substrates and high electromechanic properties. This avenue of research offers real prospects for fabrication of flexible electronic devices using printed techniques. There is no doubt of the importance and high potential of practical application of the results of studies on SAIM-assisted surface nanostructuring, although the total number of publications in this field is small due to the limited number of structuring techniques and technical character of the results.

There is a wide variety of potential applications of SAIMs in innovative microelectronic devices. The simplest relevant examples include modification of substrate surfaces, improvement of its wettability and adhesion to subsequent layers. The high-end applications include nanostructuring of surfaces and biosensorics. Rapid progress in modern microelectronics and a great variety of SAIM applications in this field pose new more sophisticated problems. Solution to these issues will undoubtedly lead to improvement of the available and to development of new energy-efficient technologies in microelectronics, to breakthrough in the diagnosis of environmental pollution and in biomedical applications and, eventually, to improvement of the quality of life.

Figures 2, 5, 12 – 15, 18, 21, 22 and 24 are courtesy of Wiley and Sons. Figures 3, 4, 10, 11, 16 and 17 are courtesy of ACS Publications. Figures 6 and 7 are courtesy of Elsevier. Figures 20 and 23 are courtesy of Springer Nature. Figure 19 is courtesy of the American Association for the Advancement of Science.

This review has been prepared within the framework of the Leading Scientific School NSh-5698.2018.3 with the financial support from the Russian Science Foundation (Project No.18-73-10182). Sections 3, 4 and 8 have been written within the framework of the State Assignment.

References

1. G.M.Whitesides, B.Grzybowski. *Science*, **295**, 2418 (2002)
2. M.Halik, H.Klauk, U.Zschieschang, G.Schmid, C.Dehm, M.Schutz, S.Maisch, F.Effenberger, M.Brunnbauer, F.Stellacci. *Nature (London)*, **431**, 963 (2004)
3. E.C.P.Smits, S.G.J.Mathijssen, P.A.van Hal, S.Setayesh, T.C.T.Geuns, K.A.H.A.Mutsaers, E.Cantatore, H.J.Wondergem, O.Werzer, R.Resel, M.Kemerink, S.Kirchmeyer, A.M.Muzafarov, S.A.Ponomarenko, B.de Boer, P.W.M.Blom, D.M.de Leeuw. *Nature (London)*, **455**, 956 (2008)
4. A.C.Hinckley, C.Wang, R.Pfattner, D.Kong, Y.Zhou, B.Ecker, Y.Gao, Z.Bao. *ACS Appl. Mater. Interfaces*, **8**, 19658 (2016)
5. A.S.Sizov, E.V.Agina, S.A.Ponomarenko. *Russ. Chem. Rev.*, **87**, 1226 (2018)
6. S.Casalini, C.A.Bortolotti, F.Leonardi, F.Biscarini. *Chem. Soc. Rev.*, **46**, 40 (2016)
7. S.A.DiBenedetto, A.Facchetti, M.A.Ratner, T.J.Marks. *Adv. Mater.*, **21**, 1407 (2009)
8. M.Halik, A.Hirsch. *Adv. Mater.*, **23**, 2689 (2011)
9. Q.Bao, S.Braun, C.Wang, X.Liu, M.Fahlman. *Adv. Mater. Interfaces*, 1800897 (2018)
10. Y.Fang, M.M.Tentzeris. In *Flexible Electronic Devices*. (Ed. S.Rackauskas). 2018. https://avxhm.se/ebooks/FlexibleElectronics18itae.html (Last accessed on 01.10. 2019)
11. D.K.Aswal, S.Lenfant, D.Guerin, J.V.Yakhmi, D.Vuillaume. *Anal. Chim. Acta*, **568**, 84 (2006)
12. A.Vilan, D.Aswal, D.Cahen. *Chem. Rev.*, **117**, 4248 (2017)
13. A.Vilan, D.Cahen. *Chem. Rev.*, **117**, 4624 (2017)
14. D.Natali, M.Caironi. *Adv. Mater.*, **24**, 1357 (2012)
15. F.Yang, S.Cheng, X.Zhang, X.Ren, R.Li, H.Dong, W.Hu. *Adv. Mater.*, **30**, 1702415 (2018)
16. J.A.Bardecker, H.Ma, T.Kim, F.Huang, M.S.Liu, Y.-J.Cheng, G.Ting, A.K.Y.Jen. *Adv. Funct. Mater.*, **18**, 3964 (2008)
17. Y.J.Lee, J.Wang, S.R.Cheng, J.W.Hsu. *ACS Appl. Mater. Interfaces*, **5**, 9128 (2013)
18. J.Wang, C.R.Friedman, W.Cabrera, K.Tan, Y.-J.Lee, Y.J.Chabal, J.W.P.Hsu. *J. Mater. Chem. A*, **2**, 15288 (2014)
19. H.-L.Yip, S.K.Hau, N.S.Baek, H.Ma, A.K.Y.Jen. *Adv. Mater.*, **20**, 2376 (2008)
20. H.Klauk, U.Zschieschang, J.Pflaum, M.Halik. *Nature (London)*, **445**, 745 (2007)
21. M.N.Kirikova, E.V.Agina, A.A.Bessonov, A.S.Sizov, O.V.Borshchev, A.A.Trul, A.M.Muzafarov, S.A.Ponomarenko. *J. Mater. Chem. C*, **4**, 2211 (2016)
22. S.G.J.Mathijssen, M.Kemerink, A.Sharma, M.Cölle, P.A.Bobbert, R.A.J.Janssen, D.M.de Leeuw. *Adv. Mater.*, **20**, 975 (2008)
23. K.Asadi, F.Gholamrezaie, E.C.P.Smits, P.W.M.Blom, B.d.Boer. *J. Mater. Chem.*, **17**, 1947 (2007)
24. J.Tsurumi, A.Y.Amin, T.Okamoto, C.Mitsui, K.Takimiya, H.Matsui, M.Halik, J.Takeya. *Org. Electron.*, **15**, 1184 (2014)
25. A.Y.Amin, A.Khassanov, K.Reuter, T.Meyer-Friedrichsen, M.Halik. *J. Am. Chem. Soc.*, **134**, 16548 (2012)
26. F.Ante, D.Kalblein, T.Zaki, U.Zschieschang, K.Takimiya, M.Ikeda, T.Sekitani, T.Someya, J.N.Burghartz, K.Kern, H.Klauk. *Small*, **8**, 73 (2012)
27. M.Salinas, C.M.Jager, A.Y.Amin, P.O.Dral, T.Meyer-Friedrichsen, A.Hirsch, T.Clark, M.Halik. *J. Am. Chem. Soc.*, **134**, 12648 (2012)
28. J.Collet, O.Tharaud, A.Chapoton, D.Vuillaume. *Appl. Phys. Lett.*, **76**, 1941 (2000)

29. S.H.Lo, D.A.Buchanan, Y.Taur, W.Wang. *IEEE Electron Device, L*, **18**, 209 (1997)
30. K.Sekine, Y.Saito, M.Hirayama, T.Ohmi. *IEEE Electron Device, T*, **48**, 1550 (2001)
31. R.T.Weitz, U.Zschieschang, F.Effenberger, H.Klauk, M.Burghard, K.Kern. *Nano Lett*., **7**, 22 (2007)
32. S.P.Schießl, F.Gannott, S.H.Etschel, M.Schweiger, S.Grünler, M.Halik, J.Zaumseil. *Adv. Mater. Interfaces*, **3**, 1600215 (2016)
33. P.H.Wöbkenberg, J.Ball, F.B.Kooistra, J.C.Hummelen, D.M.de Leeuw, D.D.C.Bradley, T.D.Anthopoulos. *Appl. Phys. Lett*., **93**, 013303 (2008)
34. K.Fukuda, T.Hamamoto, T.Yokota, T.Sekitani, U.Zschieschang, H.Klauk, T.Someya. *Appl. Phys. Lett*., **95**, 203301 (2009)
35. A.Jedaa, M.Burkhardt, U.Zschieschang, H.Klauk, D.Habich, G.Schmid, M.Halik. *Org. Electron*., **10**, 1442 (2009)
36. M.Novak, C.M.Jager, A.Rumpel, H.Kropp, W.Peukert, T.Clark, M.Halik. *Org. Electron*., **11**, 1476 (2010)
37. I.G.Hill, C.M.Weinert, L.Kreplak, B.P.van Zyl. *Appl. Phys.A*, **95**, 81 (2009)
38. D.Kalblein, R.T.Weitz, H.J.Bottcher, F.Ante, U.Zschieschang, K.Kern, H.Klauk. *Nano Lett*., **11**, 5309 (2011)
39. D.Kalblein, H.Ryu, F.Ante, B.Fenk, K.Hahn, K.Kern, H.Klauk. *ACS Nano*, **8**, 6840 (2014)
40. C.H.Lu, L.M.Qi, J.H.Yang, L.Tang, D.Y.Zhang, J.M.Ma. *Chem. Commun*., 3551 (2006)
41. M.Salinas, M.Halik. *Appl. Phys. Lett*., **102**, 203301 (2013)
42. M.Novak, T.Schmaltz, H.Faber, M.Halik. *Appl. Phys. Lett*., **98**, 81 (2011)
43. U.Kraft, M.Sejfic, M.J.Kang, K.Takimiya, T.Zaki, F.Letzkus, J.N.Burghartz, E.Weber, H.Klauk. *Adv. Mater*., **27**, 207 (2015)
44. H.Dietrich, S.Scheiner, L.Portilla, D.Zahn, M.Halik. *Adv. Mater*., **27**, 8023 (2015)
45. E.S.Cho, J.Kim, B.Tejerina, T.M.Hermans, H.Jiang, H.Nakanishi, M.Yu, A.Z.Patashinski, S.C.Glotzer, F.Stellacci, B.A.Grzybowski. *Nat. Mater*., **11**, 978 (2012)
46. H.Jinno, T.Yokota, N.Matsuhisa, M.Kaltenbrunner, Y.Tachibana, T.Someya. *Org. Electron*., **40**, 58 (2017)
47. L.Zeng, R.Turrisi, B.Fu, J.D.Emery, A.R.Walker, M.A.Ratner, M.C.Hersam, A.F.Facchetti, T.J.Marks, M.J.Bedzyk. *ACS Appl. Mater. Interfaces*, **10**, 6484 (2018)
48. Y.G.Ha, K.Everaerts, M.C.Hersam, T.J.Marks. *Acc. Chem. Res*., **47**, 1019 (2014)
49. K.Everaerts, J.D.Emery, D.Jariwala, H.J.Karmel, V.K.Sangwan, P.L.Prabhumirashi, M.L.Geier, J.J.McMorrow, M.J.Bedzyk, A.Facchetti, M.C.Hersam, T.J.Marks. *J. Am. Chem. Soc*., **135**, 8926 (2013)
50. M.de Pauli, U.Zschieschang, I.D.Barcelos, H.Klauk, A.Malachias. *Adv. Electron. Mater*., **2**, 1500402 (2016)
51. G.Ramanath, G.Cui, P.G.Ganesan, X.Guo, A.V.Ellis, M.Stukowski, K.Vijayamohanan, P.Doppelt, M.Lane. *Appl. Phys. Lett*., **83**, 383 (2003)
52. E.V.Agina, A.S.Sizov, M.Y.Yablokov, O.V.Borshchev, A.A.Bessonov, M.N.Kirikova, M.J.A.Bailey, S.A.Ponomarenko. *ACS Appl. Mater. Interfaces*, **7**, 11755 (2015)
53. P.Y.Li, F.Yang, X.C.Li, C.L.He, W.Su, J.H.Chen, L.N.Huo, R.Chen, C.S.Lu, L.F.Liang. *Appl. Surface Sci*., **280**, 164 (2013)
54. D.Chen, Y.Zhang, T.Bessho, T.Kudo, J.Sang, H.Hirahara, K.Mori, Z.Kang. *Appl. Surface Sci*., **349**, 503 (2015)
55. D.Chen, Y.Zhang, T.Bessho, J.Sang, H.Hirahara, K.Mori, Z.Kang. *Chem. Eng. J*., **303**, 100 (2016)
56. D.X.Chen, Z.X.Kang, T.Bessho. *J. Ind. Eng. Chem*., **52**, 73 (2017)
57. S.G.Mathijssen, P.A.van Hal, T.J.van den Biggelaar, E.C.Smits, B.de Boer, M.Kemerink, R.A.Janssen, D.M.de Leeuw. *Adv. Mater*., **20**, 2703 (2008)
58. K.M.Knesting, P.J.Hotchkiss, B.A.MacLeod, S.R.Marder, D.S.Ginger. *Adv. Mater*., **24**, 642 (2012)
59. H.Y.Cho, C.J.Han, I.In. *Chem. Lett*., **41**, 290 (2012)
60. C.Wu, Q.Y.Cheng, S.Q.Sun, B.H.Han. *Carbon*, **50**, 1083 (2012)
61. N.Herzer, C.Haensch, S.Hoeppener, U.S.Schubert. *Langmuir*, **26**, 8358 (2010)
62. A.Zeira, D.Chowdhury, S.Hoeppener, S.Liu, J.Berson, S.R.Cohen, R.Maoz, J.Sagiv. *Langmuir*, **25**, 13984 (2009)
63. W.Bigelow, D.Pickett, W.Zisman. *J. Colloid Sci*., **1**, 513 (1946)
64. F.N.Jones, M.E.Nichols, S.P.Pappas. *Organic Coatings: Science and Technology*. Wiley, New Jersey, 2017
65. L.Netzer, J.Sagiv. *J. Am. Chem. Soc*., **105**, 674 (1983)
66. D.Chowdhury, R.Maoz, J.Sagiv. *Nano Lett*., **7**, 1770 (2007)
67. K.Wen, R.Maoz, H.Cohen, J.Sagiv, A.Gibaud, A.Desert, B.M.Ocko. *J. ACS Nano*, **2**, 579 (2008)
68. Z.Zhang, X.Ren, B.Peng, Z.Wang, X.Wang, K.Pei, B.Shan, Q.Miao, P.K.Chan. *Adv. Funct. Mater*., **25**, 6112 (2015)
69. S.H.Lee, W.-Y.Rho, S.J.Park, J.Kim, O.S.Kwon, H.Jun. *Sci. Rep*., **8**, 16763 (2018)
70. F.Gholamrezaie, A.M.Andringa, W.S.C.Roelofs, A.Neuhold, M.Kemerink, P.W.M.Blom, D.M.de Leeuw. *Small*, **8**, 241 (2012)
71. L.L.Chua, J.Zaumseil, J.F.Chang, E.C.W.Ou, P.K.H.Ho, H.Sirringhaus, R.H.Friend. *Nature (London)*, **434**, 194 (2005)
72. J.-C.Bolsée, J.Manca. *Synth. Met*., **161**, 789 (2011)
73. S.Tanida, K.Noda, H.Kawabata, K.Matsushige. *Synth. Met*., **160**, 1574 (2010)
74. S.G.Mathijssen, M.J.Spijkman, A.M.Andringa, P.A.van Hal, I.McCulloch, M.Kemerink, R.A.Janssen, D.M.de Leeuw. *Adv. Mater*., **22**, 5105 (2010)
75. Y.Zhang, D.Ziegler, M.Salmeron. *ACS Nano*, **7**, 8258 (2013)
76. P.Lang, D.Mottaghi, P.-C.Lacaze. *Appl. Surface Sci*., **365**, 364 (2016)
77. S.Stolz, M.Scherer, E.Mankel, R.Lovrincic, J.Schinke, W.Kowalsky, W.Jaegermann, U.Lemmer, N.Mechau, G.Hernandez-Sosa. *ACS Appl. Mater. Interfaces*, **6**, 6616 (2014)
78. D.He, J.Qiao, L.Zhang, J.Wang, T.Lan, J.Qian, Y.Li, Y.Shi, Y.Chai, W.Lan, L.K.Ono, Y.Qi, J.B.Xu, W.Ji, X.Wang. *Sci. Adv*., **3**, e1701186 (2017)
79. M.T.Greiner, M.G.Helander, W.M.Tang, Z.B.Wang, J.Qiu, Z.H.Lu. *Nat. Mater*., **11**, 76 (2011)
80. J.Meyer, S.Hamwi, M.Kroger, W.Kowalsky, T.Riedl, A.Kahn. *Adv. Mater*., **24**, 5408 (2012)
81. Y.H.Zhou, C.Fuentes-Hernandez, J.Shim, J.Meyer, A.J.Giordano, H.Li, P.Winget, T.Papadopoulos, H.Cheun, J.Kim, M.Fenoll, A.Dindar, W.Haske, E.Najafabadi, T.M.Khan, H.Sojoudi, S.Barlow, S.Graham, J.L.Bredas, S.R.Marder, A.Kahn, B.Kippelen. *Science*, **336**, 327 (2012)

82. B.de Boer, A.Hadipour, M.M.Mandoc, T.van Woudenbergh, P.W.M.Blom. *Adv. Mater.*, **17**, 621 (2005)
83. P.Stoliar, R.Kshirsagar, M.Massi, P.Annibale, C.Albonetti, D.M.de Leeuw, F.Biscarini. *J. Am. Chem. Soc.*, **129**, 6477 (2007)
84. C.Albonetti, S.Casalini, F.Borgatti, L.Floreano, F.Biscarini. *Chem. Commun.*, **47**, 8823 (2011)
85. P.Tantitarntong, P.Zalar, N.Matsuhisa, K.Nakano, S.Lee, T.Yokota, K.Tajima, T.Someya. *ACS Appl. Mater. Interfaces*, **9**, 28151 (2017)
86. S.Casalini, A.Shehu, F.Leonardi, C.Albonetti, F.Borgatti, F.Biscarini. *Org. Electron.*, **14**, 1891 (2013)
87. M.M.Thuo, W.F.Reus, C.A.Nijhuis, J.R.Barber, C.Kim, M.D.Schulz, G.M.Whitesides. *J. Am. Chem. Soc.*, **133**, 2962 (2011)
88. G.Heimel, L.Romaner, J.L.Bredas, E.Zojer. *Langmuir*, **24**, 474 (2008)
89. C.Gahl, R.Schmidt, D.Brete, E.R.McNellis, W.Freyer, R.Carley, K.Reuter, M.Weinelt. *J. Am. Chem. Soc.*, **132**, 1831 (2010)
90. D.B.Habich, M.Halik, G.Schmid. *Thin Solid Films*, **519**, 7809 (2011)
91. S.A.Paniagua, A.J.Giordano, O.L.Smith, S.Barlow, H.Li, N.R.Armstrong, J.E.Pemberton, J.L.Bredas, D.Ginger, S.R.Marder. *Chem. Rev.*, **116**, 7117 (2016)
92. M.Timpel, H.Li, M.V.Nardi, B.Wegner, J.Frisch, P.J.Hotchkiss, S.R.Marder, S.Barlow, J.-L.Brédas, N.Koch. *Adv. Funct. Mater.*, **28**, 1704438 (2018)
93. H.J.Lee, A.C.Jamison, T.R.Lee. *Acc. Chem. Res.*, **48**, 3007 (2015)
94. K.Y.Wu, S.Y.Yu, Y.T.Tao. *Langmuir*, **25**, 6232 (2009)
95. M.Alt, J.Schinke, S.Hillebrandt, M.Hansel, G.Hernandez-Sosa, N.Mechau, T.Glaser, E.Mankel, M.Hamburger, K.Deing, W.Jaegermann, A.Pucci, W.Kowalsky, U.Lemmer, R.Lovrincic. *ACS Appl. Mater. Interfaces*, **6**, 20234 (2014)
96. M.F.Calhoun, J.Sanchez, D.Olaya, M.E.Gershenson, V.Podzorov. *Nat. Mater.*, **7**, 84 (2008)
97. W.T.Tsai. *Chemosphere*, **61**, 1539 (2005)
98. S.Lacher, Y.Matsuo, E.Nakamura. *J. Am. Chem. Soc.*, **133**, 16997 (2011)
99. S.Casalini, F.Leonardi, C.A.Bortolotti, A.Operamolla, O.H.Omar, L.Paltrinieri, C.Albonetti, G.M.Farinola, F.Biscarini. *J. Mater. Chem.*, **22**, 12155 (2012)
100. N.Kedem, S.Blumstengel, F.Henneberger, H.Cohen, G.Hodes, D.Cahen. *Phys. Chem. Chem. Phys.*, **16**, 8310 (2014)
101. R.Nouchi, M.Shigeno, N.Yamada, T.Nishino, K.Tanigaki, M.Yamaguchi. *Appl. Phys. Lett.*, **104**, 013308 (2014)
102. T.Abu-Husein, S.Schuster, D.A.Egger, M.Kind, T.Santowski, A.Wiesner, R.Chiechi, E.Zojer, A.Terfort, M.Zharnikov. *Adv. Funct. Mater.*, **25**, 3943 (2015)
103. M.Jesper, M.Alt, J.Schinke, S.Hillebrandt, I.Angelova, V.Rohnacher, A.Pucci, U.Lemmer, W.Jaegermann, W.Kowalsky, T.Glaser, E.Mankel, R.Lovrincic, F.Golling, M.Hamburger, U.H.Bunz. *Langmuir*, **31**, 10303 (2015)
104. M.Alt, M.Jesper, J.Schinke, S.Hillebrandt, P.Reiser, T.Rödlmeier, I.Angelova, K.Deing, T.Glaser, E.Mankel, W.Jaegermann, A.Pucci, U.Lemmer, U.H.F.Bunz, W.Kowalsky, G.Hernandez-Sosa, R.Lovrincic, M.Hamburger. *Adv. Funct. Mater.*, **26**, 3172 (2016)
105. W.E.Ford, D.Q.Gao, N.Knorr, R.Wirtz, F.Scholz, Z.Karipidou, K.Ogasawara, S.Rosselli, V.Rodin, G.Nelles, F.von Wrochem. *ACS Nano*, **8**, 9173 (2014)
106. S.Casalini, A.Shehu, S.Destri, W.Porzio, M.C.Pasini, F.Vignali, F.Borgatti, C.Albonetti, F.Leonardi, F.Biscarini. *Org. Electron.*, **13**, 789 (2012)
107. D.K.Owens, R.Wendt. *J. Appl. Polym. Sci.*, **13**, 1741 (1969)
108. S.Izawa, K.Hashimoto, K.Tajima. *Phys. Chem. Chem. Phys.*, **16**, 16383 (2014)
109. N.Shin, J.Zessin, M.H.Lee, M.Hambsch, S.C.B.Mannsfeld. *Adv. Funct. Mater.*, **28**, 1802265 (2018)
110. J.J.Kirn, S.Bachevillier, D.L.G.Arellano, B.P.Cherniawski, E.K.Burnett, N.Stingelin, C.Ayela, O.Usluer, S.C.B.Mannsfeld, G.Wantz, A.L.Briseno. *ACS Appl. Mater. Interfaces*, **10**, 26745 (2018)
111. P.Dabczynski, M.M.Marzec, L.Pieta, K.Fijalkowski, J.Raczkowska, A.Bernasik, A.Budkowski, J.Rysz. *ACS Omega*, **3**, 3631 (2018)
112. S.Piranej, D.A.Turner, S.M.Dalke, H.Park, B.A.Qualizza, J.Vicente, J.X.Chen, J.W.Ciszek. *CrystEngComm*, **18**, 6062 (2016)
113. B.Lee, Y.Chen, A.Cook, A.Zakhidov, V.Podzorov. *J. Appl. Phys.*, **116**, 144503 (2014)
114. B.Lee, A.Wan, D.Mastrogiovanni, J.E.Anthony, E.Garfunkel, V.Podzorov. *Phys. Rev. B*, **82**, 085302 (2010)
115. M.J.Panzer, C.D.Frisbie. *Appl. Phys. Lett.*, **88**, 203504 (2006)
116. J.Zessin, Z.Xu, N.Shin, M.Hambsch, S.C.B.Mannsfeld. *ACS Appl. Mater. Interfaces*, **11**, 2177 (2019)
117. M.Das Mukherjee, P.R.Solanki, G.Sumana, T.Manaka, M.Iwamoto, B.D.Malhotra. *Appl. Biochem. Biotechnol.*, **174**, 1201 (2014)
118. B.De la Franier A.Jankowski, M.Thompson. *Appl. Surface Sci.*, **414**, 435 (2017)
119. A.Syahir, K.Usui, K.-y.Tomizaki, K.Kajikawa, H.Mihara. *J. Microarrays*, **4**, 228 (2015)
120. S.Sheikh, J.C.C.Sheng, C.Blaszykowski, M.Thompson. *Chem. Sci.*, **1**, 271 (2010)
121. T.Miyata, A.Kawamura, T.Meotoiwa, M.Matsumoto, T.Uragami. *Polym. J.*, **44**, 625 (2012)
122. S.Sheikh, C.Blaszykowski, M.Thompson. *Surface Interface Anal.*, **45**, 1781 (2013)
123. M.Tyagi, A.Chandran, T.Joshi, J.Prakash, V.V.Agrawal, A.M.Biradar. *Appl. Phys. Lett.*, **104**, 154104 (2014)
124. P.Benvenuto, M.A.Neves, C.Blaszykowski, A.Romaschin, T.Chung, S.R.Kim, M.Thompson. *Langmuir*, **31**, 5423 (2015)
125. M.A.Neves, C.Blaszykowski, S.Bokhari, M.Thompson. *Biosens. Bioelectron.*, **72**, 383 (2015)
126. C.Haensch, S.Hoeppener, U.S.Schubert. *Chem. Soc. Rev.*, **39**, 2323 (2010)
127. H.Ogi, Y.Fukunishi, H.Nagai, K.Okamoto, M.Hirao, M.Nishiyama. *Biosens. Bioelectron.*, **24**, 3148 (2009)
128. R.M.Pasternack, S.R.Amy, Y.J.Chabal. *Langmuir*, **24**, 12963 (2008)
129. V.Voisin, J.Pilate, P.Damman, P.Megret, C.Caucheteur. *Biosens. Bioelectron.*, **51**, 249 (2014)
130. B.A.Prabowo, L.C.Su, Y.F.Chang, H.C.Lai, N.F.Chiu, K.C.Liu. *Sensors Actuators B*, **222**, 1058 (2016)
131. P.A.Raymundo-Pereira, F.M.Shimizu, D.Coelho, M.H.O.Piazzeta, A.L.Gobbi, S.A.S.Machado, O.N.Oliveira Jr. *Biosens. Bioelectron.*, **86**, 369 (2016)

132. B.Holzer, K.Manoli, N.Ditaranto, E.Macchia, A.Tiwari, C.Di Franco, G.Scamarcio, G.Palazzo, L.Torsi. *Adv. Biosyst.*, **1**, 1700055 (2017)
133. Z.Li, M.R.Narouz, K.Munro, B.Hao, C.M.Crudden, J.H.Horton, H.Hao. *ACS Appl. Mater. Interfaces*, **9**, 39223 (2017)
134. J.Munoz, N.Crivillers, M.Mas-Torrent. *Chemistry*, **23**, 15289 (2017)
135. T.Rahman, T.Ichiki. *Sensors (Basel)*, **17**, 2326 (2017)
136. I.Tubia, J.Paredes, E.Perez-Lorenzo, S.Arana. *Biosens. Bioelectron.*, **102**, 432 (2018)
137. J.W.Lee, S.J.Sim, S.M.Cho, J.Lee. *Biosens. Bioelectron.*, **20**, 1422 (2005)
138. C.Vericat, M.Vela, G.Benitez, P.Carro, R.Salvarezza. *Chem. Soc. Rev.*, **39**, 1805 (2010)
139. C.Perrino, S.Lee, S.W.Choi, A.Maruyama, N.D.Spencer. *Langmuir*, **24**, 8850 (2008)